Mon. Not. R. Astron. Soc. **000**, 000–000 (0000) Printed 27 October 2010 (MN LaTeX style file v2.2)

Metallicities and dust content of proximate damped Lyman alpha systems in the Sloan Digital Sky Survey

Sara L. Ellison[1], J. Xavier Prochaska[2], J. Trevor Mendel[1]
[1] *Department of Physics and Astronomy, University of Victoria, Victoria, British Columbia, V8P 1A1, Canada.*
[2] *Department of Astronomy and Astrophysics, UCO/Lick Observatory, University of California, 1156 High Street, Santa Cruz, CA 95064, USA*

27 October 2010

ABSTRACT

Composite spectra of 85 proximate absorbers (log N(H I) $\geqslant$ 20 cm^{-2} and velocity difference between the absorption and emission redshift, $\Delta V <$ 10,000 km s^{-1}) in the Sloan Digital Sky Survey are used to investigate the trends of metal line strengths with velocity separation from the QSO. We construct composites in 3 velocity bins: $\Delta V <$ 3000 km s^{-1}, 3000 < ΔV < 6000 km s^{-1} and $\Delta V >$ 6000 km s^{-1}, with further sub-samples to investigate the metal line dependence on N(H I) and QSO luminosity. Low (e.g. SiII and FeII) and high ionization (e.g. SiIV and CIV) species alike have equivalent widths (EWs) that are larger by factors of 1.5 – 3 in the $\Delta V <$ 3000 km s^{-1} composite, compared to the $\Delta V >$ 6000 km s^{-1} spectrum. The EWs show an even stronger dependence on ΔV if only the highest neutral hydrogen column density (log N(H I) $\geqslant$ 20.7) absorbers are considered. We conclude that PDLAs generally have higher metallicities than intervening absorbers, with the enhancement being a function of both ΔV and N(H I). It is also found that absorbers near QSOs with lower rest-frame UV luminosities have significantly stronger metal lines. We speculate that absorbers near to high luminosity QSOs may have had their star formation prematurely quenched. Finally, we search for the signature of dust reddening by the PDLAs, based on an analysis of the QSO continuum slopes relative to a control sample and determine a limit of E($B-V$) < 0.014 for an SMC extinction curve. This work provides an empirical motivation for distinguishing between proximate and intervening DLAs, and establishes a connection between the QSO environment and galaxy properties at high redshifts.

Key words:

1 INTRODUCTION

Damped Lyman alpha (DLA) systems with small velocity separations (typically ΔV <3000 to 5000 km s^{-1}) from the systemic redshift of the background QSO are traditionally excluded by most statistical surveys (e.g. Lanzetta et al. 1991, 1995; Wolfe et al. 1995; Storrie-Lombardi et al. 1996; Ellison et al. 2001; Peroux et al. 2001; Jorgenson et al. 2006; Ellison et al. 2008; Prochaska & Wolfe 2009; Noterdaeme et al. 2009). The logic for the ΔV criterion was originally imposed to avoid absorbers that were not representative of the intervening population (e.g. those clustered around the QSO), or directly associated with the QSO host or its outflows. A further concern for small ΔV absorbers is that proximity to the intense QSO radiation field may alter the internal ionization balance of the galactic interstellar medium (ISM). In turn, this could lead to the requirement for complex ionization corrections when converting observed column densities into elemental abundances. Despite some notable exceptions (Prochaska et al. 2002a,b; Dessauges-Zavadsky et al. 2004, 2006; Milutinovic et al. 2010), ionization corrections in intervening DLAS can generally be ignored, even when the column density is relatively low.

Although these proximity concerns have driven DLA selection criteria for two decades, there is relatively little observational evidence to support the imposition of a velocity cut. Apart from a higher incidence by a factor of ∼ 2–4 (Ellison et al. 2002; Russell, Ellison & Benn 2006; Prochaska, Hennawi & Herbert-Fort 2008), the only empirical evidence that the proximate DLAs (PDLAs) differ from the intervening absorbers has been the higher incidence of Lyα emission detected in the DLA trough (Møller & Warren 1993; Møller, Warren & Fynbo 1998; Hennawi et al. 2009). The QSO's radiation does not manifest itself in gross differences in highly ionized ISM species. For example, Fox et al. (2009) found no evidence for a more frequent occurence of NV. The CIV and OVI column densities of the proximate absorbers are also indistinguishable from the intervening population (Fox et al. 2007a, 2007b), although larger samples are needed to confirm this. It has also been concluded by Rix et al. (2007) (based on the few PDLAs with high resolution echelle spectra) that their chemical abundance patterns and overall metal enrichment are consistent with the intervening population.

We have recently re-assessed the chemical properties of PD-

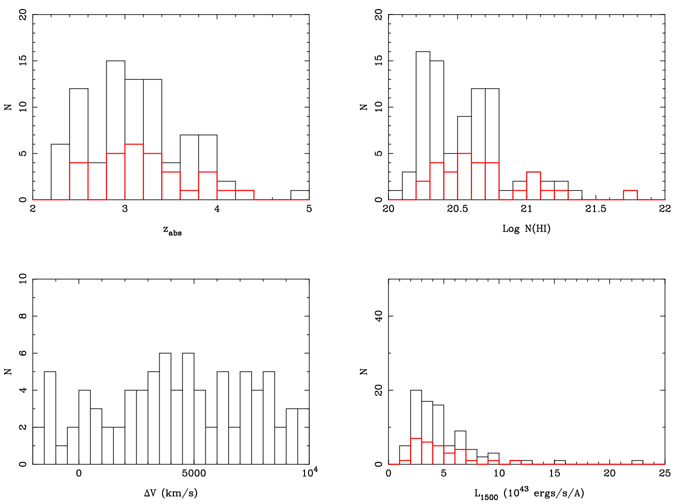

Figure 1. Distribution of absorber (absorption redshift, H I column density and velocity offset from the QSO systemic redshift) and QSO (luminosity) properties measured from the SDSS spectra for our sample of 85 PDLAs.

LAs using a sample of 16 absorbers with $\Delta V < 3000$ km s^{-1} using high resolution echelle data. In Ellison et al. (2010) we reported the first evidence that some PDLAs do exhibit both distinct metal enrichment and evidence for ionization by a hard radiation source. Specifically, it was found that although the proximate absorbers can indeed display a wide range of metallicities, at high N(H I) they are typically a factor of 3 more metal-rich than the intervening population. Although many of the proximate absorbers exhibit NV (including absorption with large velocity offsets), the most intriguing evidence for a hard radiation source came from non-solar abundances of S and Ar. Expansion of the PDLA data set is clearly required to confirm these initial findings and to understand the case-by-case dependence on QSO proximity.

In this paper, we take a complementary approach by leveraging the large statistical power of the Sloan Digital Sky Survey (SDSS). Although the majority of DLA abundance studies are performed at resolutions $R \sim 40{,}000$, with high enough S/N it is possible to detect even weak, unsaturated lines in spectra whose resolution is an order of magnitude lower (e.g. Pettini et al. 1994). Our strategy here is to construct high S/N composite spectra with various criteria (e.g. ΔV, N(H I), QSO luminosity), in order to investigate which quantities most significantly affect the metallicities of the PDLAs.

Unless otherwise stated, we assume $\Omega_M = 0.3$, $\Omega_\Lambda = 0.7$ and $H_0 = 70$ km s^{-1} Mpc^{-1}.

2 SAMPLE SELECTION

2.1 PDLA sample

The largest compilation of PDLAs is the SDSS data release (DR) 5 sample of Prochaska et al. (2008b, hereafter PHHF08). The parent sample used by PHHF08 to search for PDLAs excluded broad absorption line (BAL) QSOs and required a S/N>4 over at least one region of 20 consecutive pixels. The resulting PDLA sample contains 108 absorbers with $\Delta V < 3000$ km s^{-1} and log N(H I) > 20.3. In addition to its size, a second motivation for the adoption of the PHHF08 sample is that PHHF08 have re-computed the systemic redshifts of those QSOs with proximate absorbers, accounting for the well-known systematic blueshifts that are incurred when using rest frame UV lines such as Lyα and CIV (e.g. Gaskell 1982). Throughout this paper, we use the values of $z_{\rm abs}$ (determined from the centroid of the strongest low ion) and $z_{\rm em}$ reported by PHHF08 to compute the values of ΔV. The revised values of $z_{\rm em}$ take into account systematic shifts between the observed emission lines and those that are generally considered to be reliable estimators of the systemic value (such as Balmer and oxygen recombination lines). Uncertainties on these systematic shifts are typically a few hundred km s^{-1}. In order to explore the impact of QSO proximity on DLAs, we extend the nominal N(H I) and ΔV criteria to include proximate absorbers with log N(H I) $\geqslant 20$ and $\Delta V < 10{,}000$ km s^{-1}. These cuts are motivated by the practical limitations of SDSS's resolution and the availability of improved redshifts in PHHF08. There are 326 absorbers that fulfill the N(H I) and ΔV criteria. The sample is reduced by requiring that the spectroscopic S/N ratio in the *i*-band (as reported in the SDSS fits header) exceeds 10. We also exclude one absorber towards a BAL QSO that was not flagged in the original filter by PHHF08 (J014049.18-083942.5). The final sample consists of 85 proximate absorbers with log N(H I) $\geqslant 20$, $\Delta V <$ 10,000 km s^{-1}, S/N > 10 and improved estimates of $z_{\rm em}$ (Table 1, Figure A1). Figure 1 shows the distribution of QSO and absorber properties. 11 absorbers in the final sample have log N(H I) < 20.3. Although DLAs are more strictly absorbers with log N(H I) $\geqslant 20.3$, and 'proximate' absorbers usually considered to be within $\sim$ 3000 km s^{-1} of the QSO, for convenience, we will use the term 'PDLA' to refer to the 85 members of the sample studied in this paper.

2.2 Control sample

A handful of the strongest metal transitions can be seen in individual SDSS spectra. In order to compare the equivalent width (EW) distributions of the SiII λ 1526 line (which is not only strong but often located redwards of the Lyα forest) in the PDLAs and intervening DLA population, a sample of 85 intervening DLAs is assembled as a control sample. The control sample is drawn from the DR5 DLA catalogue of Prochaska & Wolfe (2009), supplemented with a non-statistical sample of lower column density absorbers (recall that the PDLA sample extends to log N(H I) = 20). For each PDLA, the intervening DLA which is the closest simultaneous match in $z_{\rm abs}$, N(H I) and QSO fibre *i* magnitude is determined. The fibre magnitude criterion is included in the matching process so that a similar spectral S/N is achieved. Once a match is made, the intervening DLA is not replaced and can not be considered as a match for a different PDLA. We also require that the SiII λ 1526 line is redwards of the QSO's Lyα line, i.e. $z_{\rm em} < 1.255 \times (1 + z_{\rm abs}) - 1$. A Kolmogorov-Smirnov test (KS) is performed to ensure that the control sample properties are well matched to the PDLAs. The KS probabilities are 92% ($z_{\rm abs}$), 83% (N(H I)) and 98% (*i* magnitude) indicating that there is no difference in the distribution of these properties between the DLAs and PDLAs.

A second control sample is constructed in order to assess the extinction properties of the PDLAs via the comparison on the spectral slopes of QSOs with and without PDLAs (Section 5). The control sample is drawn from the list of DR5 QSOs with $z > 2$, no PDLA and no strong BAL features, as determined from visual inspection. We do not exclude QSOs with intervening DLAs because

QSO	*i* mag	Plate	MJD	Fibre	z_{em}	z_{abs}	log N(H I)	ΔV (km s^{-1})
J012747.80+140543.2	18.56	0425	51898	278	2.4877	2.4416	20.30	3991.57
J014214.74+002324.3	18.08	0401	51788	500	3.3734	3.3481	20.40	1733.61
J023903.43-003850.8	18.71	0408	51821	134	3.0782	3.0185	20.35	4371.54
J025518.58+004847.6	18.87	0410	51816	466	3.9936	3.9145	21.40	4771.41
J073718.16+323631.5	19.10	0541	51959	151	3.0175	2.8926	20.30	9487.00
J075901.28+284703.4	19.02	0859	52317	453	2.8550	2.8223	21.05	2532.00
J080050.28+192058.9	18.89	1922	53315	152	3.9533	3.9465	20.25	448.52
J081240.68+320808.6	17.43	0861	52318	333	2.7045	2.6259	21.30	6391.40
J081256.05+563746.9	18.80	1872	53386	474	3.3170	3.2251	20.00	6425.95
J081256.05+563746.9	18.80	1872	53386	474	3.3170	3.3387	20.35	-1310.54
J081518.56+291153.9	19.33	0930	52618	593	4.2552	4.2588	20.50	-205.44
J082107.61+310751.2	17.04	0931	52619	491	2.6193	2.5347	20.15	7060.41
J082531.88+263619.2	18.93	1267	52932	051	2.5640	2.5409	20.45	1933.80
J082612.54+451355.7	19.16	0548	51986	167	3.8170	3.7068	20.50	6979.90
J082638.59+515233.2	17.02	0442	51882	528	2.8438	2.8333	20.80	820.62
J083510.92+065052.8	18.37	1297	52963	517	3.9781	3.9556	20.35	1359.00
J083914.14+485125.7	18.64	0550	51959	460	2.9673	2.9692	20.60	-136.08
J090017.61+490001.9	18.72	0765	52254	306	3.2080	3.2054	20.95	185.42
J090033.49+421546.8	16.78	0831	52294	201	3.2954	3.2456	20.30	3477.11
J090940.67+330347.6	18.51	1272	52989	022	3.7835	3.6583	20.60	7922.54
J091210.35+054742.0	18.09	1194	52703	257	3.2407	3.1231	20.35	8398.34
J091223.02+562128.5	18.75	0451	51908	312	2.9816	2.8894	20.55	7027.37
J091548.90+302542.6	18.85	1936	53330	614	3.1928	3.0678	20.45	9091.90
J092914.49+282529.1	17.54	1940	53383	441	3.4044	3.2629	21.10	9743.62
J093019.58+423803.9	18.86	0870	52325	042	3.7363	3.6098	20.20	8119.55
J094453.89+372840.2	18.81	1276	53035	172	3.3397	3.3356	20.45	262.81
J095256.41+332939.0	18.74	1945	53387	032	3.3962	3.3468	20.70	3369.33
J095744.46+330820.7	18.15	1948	53388	137	4.2088	4.1794	20.45	2039.99
J095817.81+494618.3	18.64	1006	52708	474	2.3555	2.2909	20.65	5831.18
J095937.11+131215.4	17.43	1744	53055	368	4.0717	3.9131	20.15	9540.28
J100409.35+120256.5	18.87	1744	53055	109	2.8804	2.8006	20.60	6232.89
J101725.88+611627.5	18.13	0771	52370	155	2.8069	2.7681	20.60	3073.19
J102611.35+341459.9	18.45	1958	53385	449	3.3991	3.4141	20.60	-1021.19
J102619.09+613628.8	18.43	0772	52375	227	3.8442	3.7853	20.35	3657.30
J103403.87+380248.4	18.15	1998	53433	343	3.5605	3.5161	20.70	2948.23
J104837.40-002813.6	19.28	0276	51909	313	4.0070	3.8880	20.65	7214.72
J105123.03+354534.3	18.54	2090	53463	105	4.8990	4.8208	20.40	4003.30
J110855.47+120953.3	18.62	1604	53078	383	3.6737	3.5453	20.75	8302.28
J111151.60+133235.9	17.15	1752	53379	242	2.4328	2.3820	20.30	4401.43
J111611.73+411821.5	18.04	1439	53003	595	2.9829	2.9426	20.20	3012.79
J113002.34+115438.3	18.39	1606	53055	102	3.3939	3.3171	20.20	5226.94
J113008.19+535419.8	17.60	1014	52707	211	3.0495	2.9870	20.25	4575.67
J113130.41+604420.7	17.60	0776	52319	250	2.9069	2.8755	20.50	2428.55
J113354.89+022420.9	18.92	0513	51989	428	3.9865	3.9147	20.65	4332.45
J115526.34+351052.6	18.85	2035	53436	011	2.8374	2.7582	20.70	6247.59
J120359.07+341114.2	18.58	2099	53469	635	3.7484	3.6740	20.60	4718.10
J120359.07+341114.2	18.58	2099	53469	635	3.7484	3.6860	20.60	3917.08
J121324.58+423538.5	18.85	1450	53120	455	3.7663	3.7646	20.60	56.65
J122040.23+092326.8	18.05	1230	52672	066	3.1462	3.1322	20.75	978.39
J123840.93+343703.3	18.44	2020	53431	490	2.5718	2.4712	20.80	8551.19
J123937.56+343701.8	18.41	2020	53431	501	2.4632	2.4812	21.10	-1727.50
J124138.32+461717.0	18.57	1455	53089	257	2.7697	2.6672	20.70	8300.70
J124640.37+111302.9	18.02	1694	53472	085	3.1475	3.0975	20.45	3594.52
J125659.47+301439.0	18.71	2011	53499	388	2.9457	2.8805	20.70	4967.33
J125759.22-011130.2	18.64	0293	51994	127	4.1120	4.0208	20.30	5358.04
J125832.14+290903.1	18.95	2011	53499	171	3.4830	3.3512	20.55	8928.92
J130152.57-030729.3	18.47	0339	51692	277	3.0706	3.0510	20.50	1336.92
J130426.15+120245.5	17.93	1696	53116	278	2.9775	2.9135	20.55	4835.33
J130426.15+120245.5	17.93	1696	53116	278	2.9775	2.9289	20.35	3726.19
J132235.12+584124.6	18.63	0959	52411	237	2.8507	2.8183	20.50	2511.27

Table 1. 85 PDLAs used in this study. Magnitudes are in the Petrosian system and are corrected for Galactic extinction.

QSO	*i* mag	Plate	MJD	Fibre	z_{em}	z_{abs}	log N(H I)	ΔV (km s^{-1})
J133724.69+315254.5	18.54	2109	53468	052	3.1829	3.1742	21.30	617.43
J135305.18-025018.2	18.70	0914	52721	235	2.4149	2.3618	20.30	4647.59
J135317.11+532825.5	18.29	1043	52465	492	2.9153	2.8346	20.80	6192.41
J135803.97+034936.0	18.62	0856	52339	196	2.8937	2.8535	20.40	3113.30
J135842.92+652236.6	18.70	0498	51984	398	3.1731	3.0641	20.30	7576.96
J135936.21+483923.1	18.44	1671	53446	305	2.3641	2.2572	20.40	9647.59
J141906.32+592312.3	17.69	0789	52342	368	2.3189	2.2467	20.95	6597.23
J141950.54+082948.2	18.66	1811	53533	198	3.0344	3.0504	20.40	-1157.78
J142446.29+054717.3	17.91	1827	53531	269	2.3944	2.3072	20.40	7751.38
J144127.66+475048.8	18.80	1674	53464	608	3.1977	3.2130	21.05	-1091.46
J145329.53+002357.5	18.49	0309	51994	423	2.5417	2.4436	20.40	8389.79
J145429.65+004121.2	19.42	0309	51994	466	2.6567	2.5657	20.15	7667.94
J150726.32+440649.2	17.80	1677	53148	424	3.1133	3.0642	20.75	3595.06
J152413.35+430537.4	18.86	1678	53433	614	3.9196	3.8809	20.70	2399.96
J154153.46+315329.4	17.53	1581	53149	220	2.5530	2.4434	20.85	9388.11
J155814.51+405337.0	18.85	1054	52516	602	2.6403	2.5521	20.30	7356.66
J160413.97+395121.9	17.95	1055	52761	459	3.1542	3.1625	21.75	-656.45
J164716.62+313254.4	18.53	1341	52786	025	2.5173	2.4936	20.25	2028.25
J170353.98+362439.6	18.91	0820	52438	631	2.4764	2.4186	20.25	5046.92
J173935.27+575201.7	19.06	0358	51818	605	3.2081	3.1357	20.35	5242.13
J210025.03-064146.0	18.21	0637	52174	370	3.1295	3.0918	21.05	2729.34
J211443.94-005532.7	18.68	0986	52443	185	3.4245	3.4420	20.50	-1211.24
J223843.56+001647.9	19.02	0377	52145	560	3.4499	3.3654	20.40	5750.84
J231543.56+145606.4	18.58	0745	52258	355	3.3769	3.2735	20.30	7149.85
J232115.48+142131.5	18.44	0745	52258	232	2.5539	2.5729	20.60	-1607.98

Table 1. Continued. 85 PDLAs used in this study.

the PDLA sample will have the same statistical occurence of intervening absorbers. In order to reduce the statistical uncertainty in the properties of our control sample, multiple control spectra are matched to each PDLA spectrum. The best match for each QSO with a PDLA in absolute Petrosian *i* magnitude and z_{em} is taken from the list of non-PDLA QSOs (without replacement) resulting in a sample of 85 control QSOs. The KS probabilities that the *i* magnitudes and z_{em} of the PDLA and control QSOs are drawn from the same distribution are calculated. The process is repeated, with each iteration taking the next best simultaneous match in *i* and z_{em} until the KS probability of one of the two quantities drops below 30%. This process yields 20 control QSOs for every PDLA QSO.

3 COMPOSITE SPECTRA

Before creating data stacks, the absorption redshift determined by PHHF08 was checked by fitting gaussians to three transitions in the SDSS spectra, where detected: OI λ1302, SiII λ1304 and SiII λ1526. The average of the metal line redshifts was adopted for spectral stacking. The mean offset between the values reported by PHHF08 and our mean metal line redshifts is 0.0002±0.001, where 0.001 corresponds to 75 km s^{-1} at z=3. The SDSS pixel scale is 69 km s^{-1} per pixel, so the typical shifts are $\ll$ 1 pixel. As stated above, the ΔV values are still calculated based on the PHHF08 redshifts for easy reference and comparison to that work.

All of the spectra are shifted to the rest-frame of the proximate absorber as determined from the metal lines or using the original Lyα redshift in 3 cases where no metals were detected. The spectra are normalized using continua that are fit using the Starlink software DIPSO. Composites are made by median combining the individual normalized, rest-frame spectra. Using the median has three advantages over a mean combination. First, the median is more robust against spurious spectral features and a small number of absorbers with extreme absorption properties. Second, the unabsorbed continuum has a value very close to unity in the median composite. The mean composite is affected by other absorption (at different redshifts) resulting in a continuum level noticably below unity. Nonetheless, we have performed the analyses in this paper for both mean and median composites and the basic conclusions are unchanged. Figure 2 shows the stack of all 85 absorbers. The composite has a S/N ~ 150 at <2000 Å, decreasing to ~60 at 2500 Å. Note the different *y*-axis scales in the different panels to accentuate absorption feature detections. The S/N is high enough to detect relatively weak species such as SiII λ 1808, NiII λ 1741 and ZnII λ 2026.

In Figure 3 we divide the sample into three approximately equal-sized samples based on ΔV. The cuts are made at ΔV < 3000 km s^{-1} (29 absorbers), 3000 < ΔV < 6000 (27 absorbers) and 6000 < ΔV < 10,000 km s^{-1} (29 absorbers). The median N(H I) of the absorbers in each of the velocity sub-samples is 20.6, 20.4 and 20.5 respectively. PHHF08 quote typical N(H I) errors of 0.15–0.20 dex, indicating that the ΔV sub-sample differences are not significant. We also compare each of the samples with a Kolmogorov-Smirnov test and confirm that there is no statistical distinction in the N(H I) distributions. The velocity sub-samples are further divided by N(H I). When dividing by N(H I) we do not aim to equalize the number of spectra contributing to each composite. Instead, we are motivated by the physical distinction that might arise as the ISM of the proximiate absorbers becomes more shielded. In Figures 5 and 6 we show the composite spectra of QSOs with log N(H I) < 20.7 and log N(H I) $\geqslant$ 20.7 absorbers respectively [for clarity, only the lowest (ΔV < 3000 km s^{-1}) and highest (ΔV > 6000 km s^{-1}) velocity sub-samples are shown].

Assuming that the N(H I) distributions of the three ΔV samples

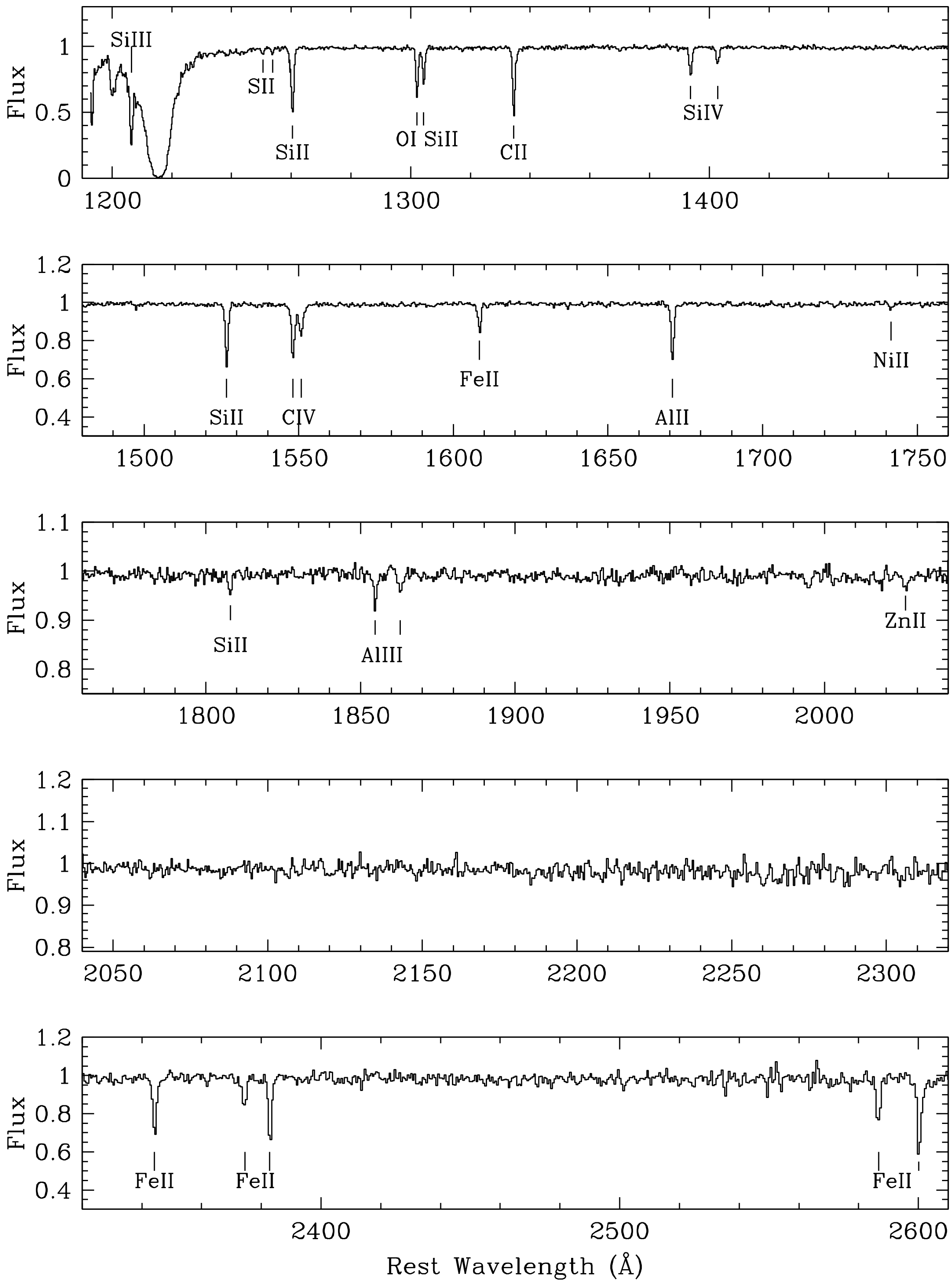

Figure 2. Median-combined composite spectrum of 85 proximate absorbers with $N(\text{H I}) \geqslant 20$ and $\Delta V < 10{,}000$ km s^{-1}. The *x*-axis is in the absorber rest-frame. Note the different *y*-axis scales in the different panels to accentuate absorption feature detections.

Sample	# Absorbers	SII λ1253 (mÅ)	OI λ1302 (mÅ)	SiIV λ1393 (mÅ)	SiII λ1526 (mÅ)	CIV λ1548 (mÅ)	FeII λ1608 (mÅ)	Z ($Z_\odot$)	$< z_{abs} >$
All	85	37±3	368±8	242±6	366±8	357±8	180±6	1/34	3.18
$\Delta V < 3000$ km s^{-1}	29	45±5	461±15	375±5	455±5	710±7	293±11	1/25	3.25
$3000 < \Delta V < 6000$ km s^{-1}	27	36±4	385±10	220±10	345±7	308±5	171±7	1/37	3.23
$\Delta V > 6000$ km s^{-1}	29	...	332±10	203±5	313±6	217±7	145±5	1/43	3.07
$\Delta V < 3000$ km s^{-1}, N(H I)<20.7	18	49±10	395±15	358±8	344±12	641±10	180±10	1/37	3.30
$3000 < \Delta V < 6000$ km s^{-1}, N(H I)<20.7	23	30±9	370±13	230±15	372±10	339±10	156±15	1/34	3.21
$\Delta V > 6000$ km s^{-1}, N(H I)<20.7	20	...	320±15	239±13	326±15	244±10	121±10	1/40	3.16
$\Delta V < 3000$ km s^{-1}, N(H I)$\geqslant$20.7	11	51±6	800±26	430±13	787±12	750±20	383±15	1/12	3.15
$3000 < \Delta V < 6000$ km s^{-1}, N(H I)$\geqslant$20.7	4	41±7	441±15	102±20	297±20	315±25	225±20	1/48	3.36
$\Delta V > 6000$ km s^{-1}, N(H I)$\geqslant$20.7	9	...	295±10	120±14	304±6	164±10	177±7	1/45	2.86
$\Delta V < 3000$ km s^{-1}, $L_{1500} < 4 \times 10^{43}$	14	60±10	532±17	415±21	500±15	735±20	325±23	1/22	2.99
$\Delta V < 3000$ km s^{-1}, $L_{1500} > 4 \times 10^{43}$	15	<120	455±20	306±13	355±15	695±15	242±20	1/36	3.49

Table 2. Rest-frame equivalent widths for the full composite sample and three ΔV sub-samples. The penultimate column indicates the metallicity as a fraction of the solar value, according to the EW(SiII λ1526)-metallicity relation of Prochaska et al. (2008a). The top line refers to the composite shown in Figure 2. The second section refers to the 3 ΔV composites shown in Figure 3. The third section refers to the low and high ΔV samples with low N(H I) shown in Figure 5. The fourth section refers to the low and high ΔV samples with high N(H I) shown in Figure 6. The fifth section refers to cuts in QSO luminosity shown in Figure 7.

are comparable, for a given metallicity the EWs of the various metal species should also be comparable in the absence of any proximity effects. From Figure 3 it is visually striking that the majority of absorption lines are strongest in the lowest ΔV composite. This is investigated quantitatively by measuring absorption line equivalent widths. EWs are determined using single gaussian fits within IRAF's SPLOT task. For the CIV $\lambda\lambda$1548, 1550 doublet the deblending option was used since the lines have mild overlap in stacks with the highest CIV EWs. Deblending was also necessary for the OI λ 1302 transition in some of the composites (where blending with SiII λ 1304 was evident). The rest-frame EW of several detected transitions are given in Table 2 and Figure 4 provides a further visual representation of how the EWs vary as a function of ΔV. In most cases, errors in continuum placement dominate over statistical error. The EW errors listed in Table 2 reflect the range of values obtained over multiple fit realizations rather than the formal error from the random noise.

4 RESULTS FROM COMPOSITE SPECTRA

4.1 Metallicity indicators

SiII and FeII are commonly used as indicators of DLA metallicity due to the relatively large number of observable transitions with a range of oscillator strengths. The FeII λ1608 line is often unsaturated in intervening DLAs. For comparable N(H I) distributions in the three sub-samples, and under the assumption that the line is unsaturated, the EW of FeII λ1608 can therefore be used as a relative metallicity indicator. From Table 2 we see that the EW of FeII λ1608 is twice as large in the $\Delta V < 3000$ km s^{-1} sample than the $\Delta V > 6000$ km s^{-1} composite. For PDLAs with $3000 < \Delta V < 6000$ km s^{-1} the strength of FeII λ1608 is intermediate between the two samples, being $\sim$ 20% larger than measured in the high ΔV composite. Figure 3 shows that the same trend is present for other FeII lines. The mean absorption redshifts of the composite spectra are given in Table 2 in order to indicate any effects that might be attributed to metallicity evolution. As a guide, Dessauges-Zavadsky

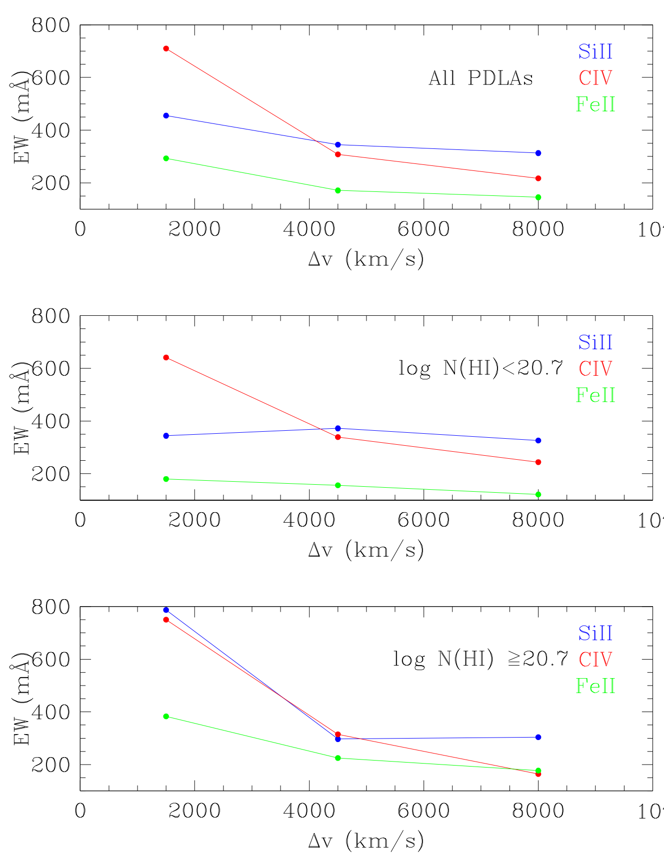

Figure 4. For three different absorption species, the rest-frame equivalent width is plotted as a function of ΔV. The top panel shows measurements from the composite spectra of the full PDLA sample (see also the second section in Table 2). The middle and lower panels show the EWs measured in the composite of spectra of the low and high N(H I) sub-samples respectively (third and fourth sections fo Table 2).

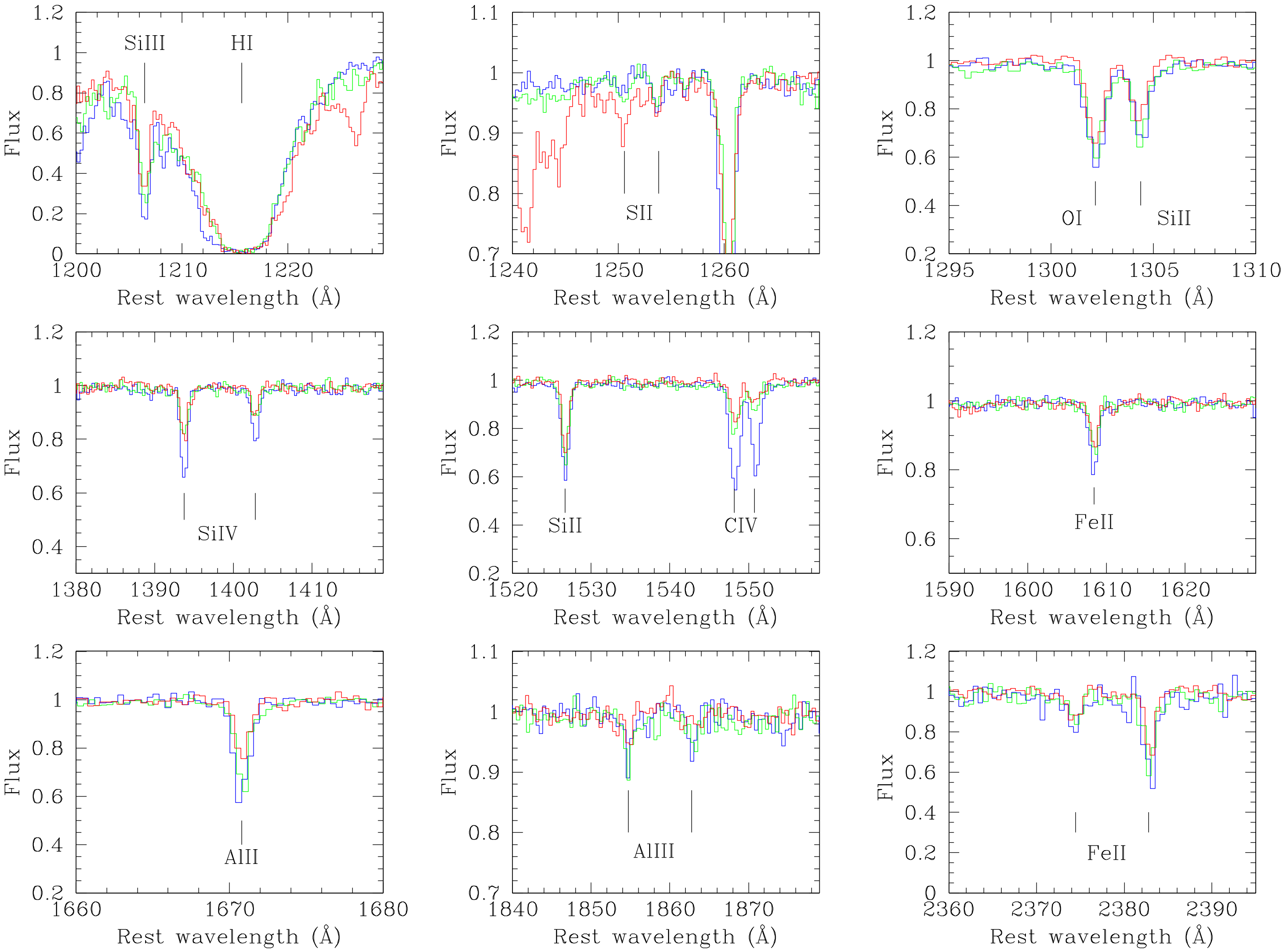

Figure 3. Median-combined composite spectrum of proximate absorbers $N(\text{H I}) \geqslant 20$ split by ΔV: $\Delta V < 3000$ km s^{-1} (blue), $3000 < \Delta V < 6000$ km s^{-1} (green), $\Delta V > 6000$ (red) km s^{-1}. The panels show the strongest absorption features visible in the full composite shown in Figure 2.

et al. (2009) find that the [Fe/H] in DLAs changes by 0.19 dex per unit redshift.

Although almost always saturated, the EW of SiII λ1526 can also be used as a metallicity diagnostic. The EWs of heavily saturated metal lines yield information about the velocity spread of the absorption (Ellison 2006; Ellison et al. 2008), which in turn is expected to correlate with mass. Murphy et al. (2007) and Nestor et al. (2003) have both found that there is a correlation between MgII EW and metallicity, and even unsaturated metal lines appear to exhibit a correlation between velocity spread and metallicity (e.g. Ledoux et al. 2006). Prochaska et al. (2008a) have calibrated the relationship between EW(SiII λ1526) and metallicity over two orders of magnitude from 1/300 to 1/3 solar. For the values of EW (SiII λ1526) in Table 2 the calibration of Prochaska et al. (2008a) yields metallicities of 1/25, 1/37 and 1/43 of the solar value for the low, intermediate and high ΔV samples respectively. If no ionization corrections are needed, the FeII and SiII lines indicate that the metallicity of PDLAs with $\Delta V < 3000$ km s^{-1} are typically twice as high as absorbers with $6000 < \Delta V < 10{,}000$ km s^{-1}.

We now consider the metal line strengths within the same velocity cuts, but now we additionally divide the sample by H I column density (Figures 5 and 6). When only the log $N(\text{H I}) < 20.7$ absorbers are included in the stack, the EW of FeII λ1608 is only 50% larger in the low ΔV sample than the high ΔV composite (compared to a factor of 2 for the full stack). The EW of SiII λ 1526 indicates metallicities of 1/37 and 1/40 solar for the $\Delta V < 3000$ km s^{-1} and $\Delta V > 6000$ km s^{-1} respectively. The only species whose EW increases by more than 50% in the $\Delta V < 3000$ km s^{-1} spectrum is CIV (see middle panel of Figure 4). Conversely, there is a much larger difference in the strengths of *all* of the metal lines when only absorbers with log $N(\text{H I}) \geqslant 20.7$ are included in the composite. This result is visually striking in Figure 6. The larger difference between EWs in the low and high velocity stacks with log $N(\text{H I}) \geqslant 20.7$ is caused mostly by a large increase (often a factor of two) in the EWs of transitions in the former. This is true of both low ionization species such as SiII λ 1526 and high ionization species such as CIV λ 1548. The EWs of both of these elements are known to scale with metallicity (Fox et al. 2007a; Prochaska et al. 2008a). Using

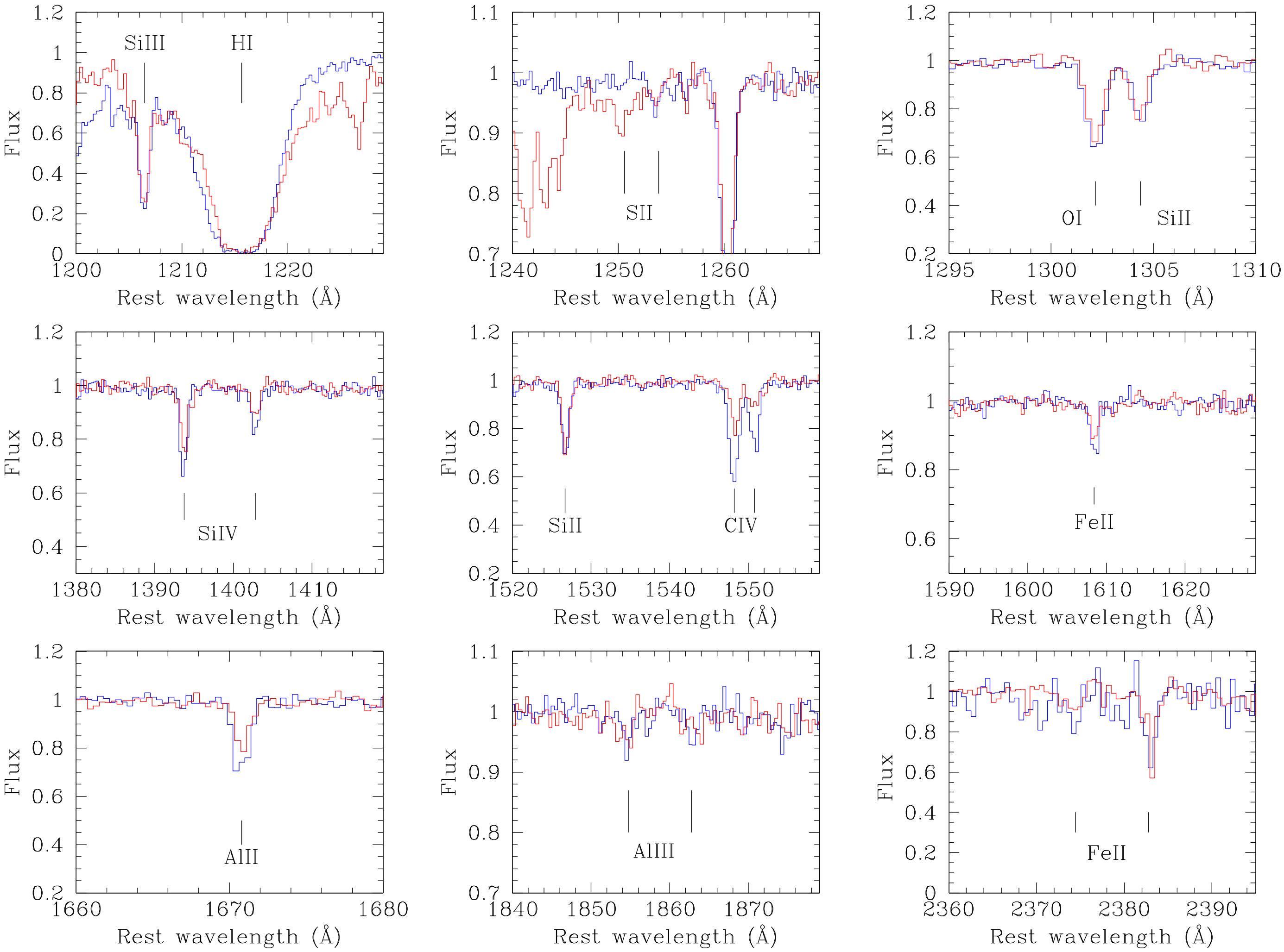

Figure 5. Median-combined composite spectrum of proximate absorbers with $20 < N(\text{H I}) < 20.7$ split by ΔV: $\Delta V < 3000$ km s^{-1} (blue), and $\Delta V > 6000$ (red) km s^{-1}. The panels show the strongest absorption features visible in the full composite shown in Figure 2. These are the same transitions shown in Figure 3.

the calibration of Prochaska et al. (2008a), the SiII λ 1526 EWs indicate metallicities of 1/12 and 1/45 solar for the low and high ΔV ($N(\text{H I}) \geqslant 20.7$) composites respectively, even though the former has a slightly higher mean redshift (3.15 compared to 2.86, see Table 2). This is consistent with the finding of Ellison et al. (2010) that the PDLAs have a higher metallicity than the intervening population when the $N(\text{H I})$ is large. However, the difference between EWs in the low and high velocity stacks with log $N(\text{H I}) \geqslant 20.7$ (Figure 6) is exagerated in the case of CIV and SiIV, whose EWs in the high ΔV composites significantly *decrease* at higher $N(\text{H I})$. The lower column densities of CIV and SiIV in the higher $N(\text{H I})$ composite (for $\Delta V > 6000$ km s^{-1}) is surprising. At these relative velocities we would consider these systems to be largely intervening and Fox et al. (2007a) found that there is no trend between N(CIV) and $N(\text{H I})$ in intervening DLAs. However, at CIV column densities above $\sim$ 14.5 the doublet becomes saturated and only a lower limit can be derived, a fairly common situation for DLAs (Fox et al. 2007a). Since Fox et al. (2007a) show that both the column density and velocity spread of CIV correlate with metallicity, the lower EW(CIV) at high $N(\text{H I})$ and high ΔV may be another manifestation of the paucity (at intervening redshifts) of high metallicity absorbers with high $N(\text{H I})$ (e.g. Schaye 2001; Krumholz et al. 2009).

4.2 Ionization indicators

Ellison et al. (2010) suggested that sub-solar SII/SiII ratios may be an indicator of a hard ionizing source. SII is usually studied via the triplet at 1250, 1253 and 1259 Å. In the SDSS data, the strongest line (λ 1259) is blended with the SiII λ 1260 line. The next strongest line (λ 1253) is clearly detected in our 3 ΔV composites, but there may be some contribution from Lyα absorption in the $\Delta V > 6000$ km s^{-1} sample. We therefore only consider the SII λ 1253 absorption in the low and intermediate velocity samples. Table 2 shows that although the low ΔV composite has a slightly higher (by 9 mÅ) EW, the measurements are consistent within the errors. If the silicon abundance is $\sim$ 50% higher in the low ΔV sample, the sulphur EWs indicate that the $\Delta V < 3000$ km s^{-1} PDLAs have a SII/SiII ratio 50% lower than the $3000 < \Delta V < 6000$ km s^{-1} sample.

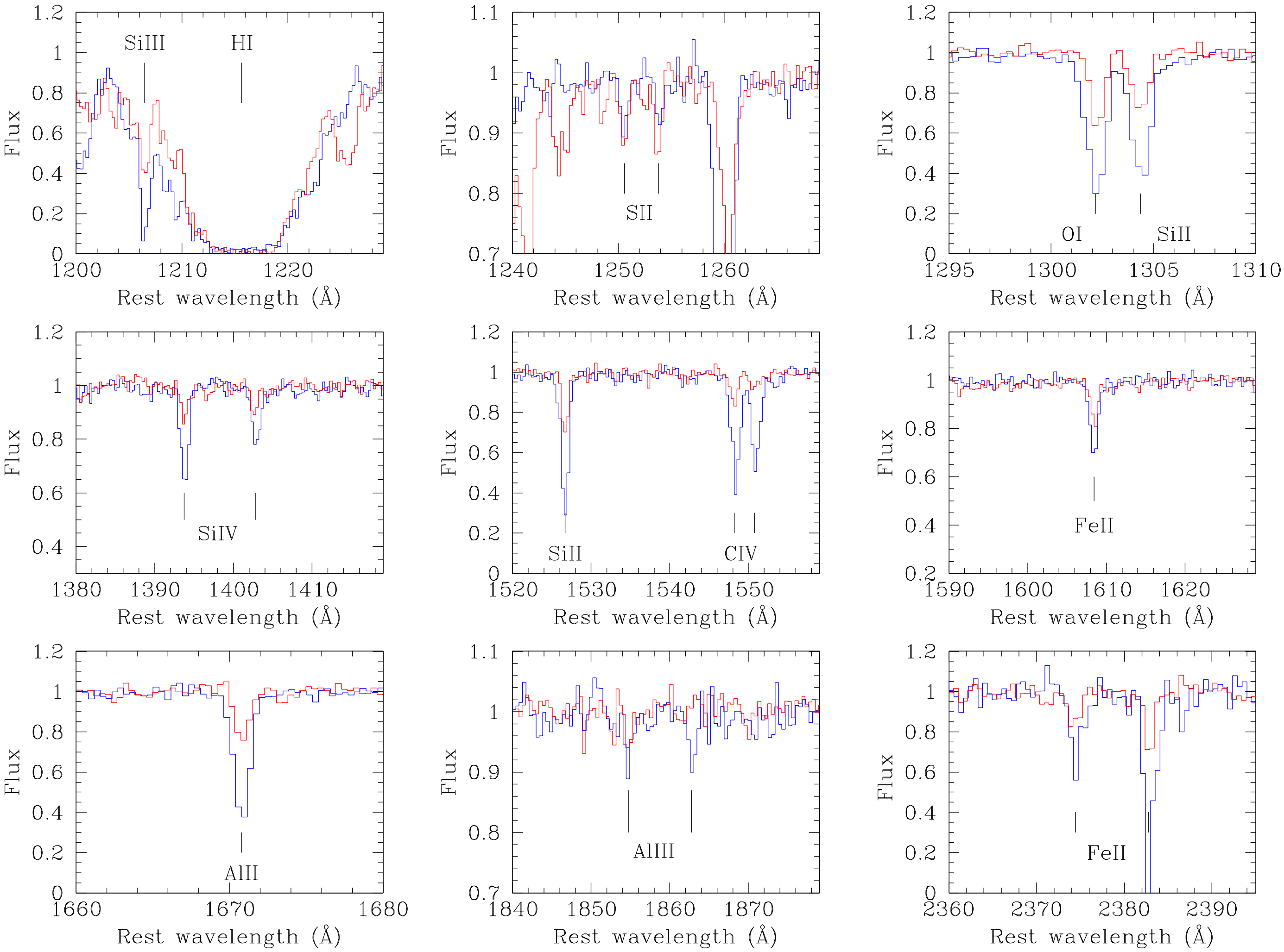

Figure 6. Median-combined composite spectrum of proximate absorbers with $N(\mathrm{H\,I}) \geqslant 20.7$ split by ΔV: $\Delta V < 3000$ km s^{-1} (blue), and $\Delta V > 6000$ (red) km s^{-1}. The panels show the strongest absorption features visible in the full composite shown in Figure 2. These are the same transitions shown in Figure 3.

Similarly, the SiII EW in the $N(\mathrm{H\,I}) \geqslant 20.7$ composite (third section of Table 2) has increased by a factor of 2.5 at low ΔV, whereas the SII EW has increased by only 20% (and is actually consistent with the $3000 < \Delta V < 6000$ km s^{-1} sample within the errors). Higher SII/SiII ratios in PDLAs are consistent with the trend identified by Ellison et al. (2010). However, the relatively large uncertainties on the SII EWs mean that this result should be regarded as tentative.

The species which exhibits the most striking difference between the 3 ΔV composites is CIV. There is more than a factor of three difference between the EW of CIV λ 1548 in the low and high ΔV composite spectra. This factor is even larger when only the log $N(\mathrm{H\,I}) \geqslant 20.7$ are included in the stack, where the EW in the low ΔV spectrum is almost a factor of 6 larger than the $\Delta V >$ 6000 km s^{-1} composite. The difference between the low and high ΔV samples is much smaller for the low $N(\mathrm{H\,I})$ absorbers, only a factor of ~ 2.5. We see a similar behaviour for the SiIV EWs: a factor of ~ 3.5 difference between low and high ΔV composites when log $N(\mathrm{H\,I}) \geqslant 20.7$, but only 50% difference for the low $N(\mathrm{H\,I})$ stack. This is ostensibly surprising, as one might expect the lower $N(\mathrm{H\,I})$ absorbers to be more susceptible to ionization effects, whereas high $N(\mathrm{H\,I})$ absorbers might remain shielded even if they are relatively close to the QSO.

NV is observed in the low ΔV composite but unfortunately can not be compared to the intermediate or high velocity spectra, because of blending by the Lyα forest. However, Ellison et al. (2010) have argued that strong NV in PDLAs may be at least partly due to higher metallicity, rather than (entirely) due to enhanced ionization (see also Fox et al. 2009).

4.3 Dependence on QSO luminosity

We investigate the effect of QSO luminosity on the composite spectra by dividing the sample of $\Delta V < 3000$ km s^{-1} absorbers (of which there are 29) in half, based on the QSO flux at λ=1500 Å in the QSO rest-frame. The median luminosity used to divide the QSOs into 'low' and 'high' luminosity samples is 4×10^{43} ergs/s/Å. The profiles of prominent absorption lines are shown for the low and high luminosity composites in Figure 7. The EWs of selected transitions are given in Table 2. The EWs of the low and high ionization species alike are larger in the lower QSO luminosity composite, despite an excellent agreement in the median N(H I) values of the two samples (20.6 and 20.5) and a KS test probability of 86% that they are drawn from the same distribution. The difference in the profiles in Figure 7 is therefore not due to different N(H I) distributions and is also unlikely to be due to an ionization effect for several reasons. First, OI is expected to be robust against ionization effects (e.g. Vladilo et al. 2001). Second, in the presence of either a hard (QSO) or a soft (stellar) ionizing spectrum, metallicities derived from SiII or FeII are expected to be over-estimated (Howk & Sembach 1999; Vladilo et al. 2001; Rix et al. 2007). Third, Ellison et al. (2010) show that [S/H] is under-estimated by at least a factor of three in more than half of the N(H I) < 20.7 PDLAs in their high resolution study, yet the SII EWs in the low and high flux composites are consistent within the errors.

York et al. (2006) and Vanden Berk et al. (2008) conducted a similar analysis to ours, constructing composite spectra from SDSS data of MgII absorbers at intervening and proximate velocities, respectively. When their samples were divided by QSO magnitude (at i = 19.1 and M_i = 26.5, for the two studies) the faint QSO composite was found to have stronger metal lines for both intervening and proximate absorbers. It was concluded that this effect was likely due to a selection bias since weaker MgII systems are typically only detected towards brighter QSOs. The (mean) composite spectra of the bright and faint samples were therefore not constructed of absorbers with the same MgII EW distribution.

Such a bias is not likely to affect our selection of PDLAs. First, the identification of a PDLA relies on the broad, saturated Lyα which is easily detected in spectra with much lower S/N than we require here (recall that PHHF08 required a S/N> 4, but our criterion is an i band S/N > 10). Second, we have checked that the N(H I) distributions of the low and high luminosity samples are consistent. This can be seen visually in the top left panel of Figure 7 and is confirmed with a KS test (described above). Therefore, although we might expect the overall S/N of our low luminosity composite to be lower, this does not affect the EW of the metal lines we measure in our median composite. Nonetheless, we check explicitly that the dependence of PDLA EWs on QSO luminosity is not due to a bias by constructing composites of ΔV >6000 km s^{-1} absorbers again split by QSO luminosity. The EWs of the low and high ionization lines are now largely consistent with each other, as might be expected for these absorbers, which most studies would consider as intervening. However, a quantitative comparison of the low vs. high luminosities compsites of the ΔV> 6000 km s^{-1} sample is hampered by a non-negligible difference in the typical H I column densities. Both the median and mean N(H I) values differ by ~ 0.3 dex with a KS probability of only 6% that they are drawn from the same population.

It is not clear why the PDLAs should have higher metal line EWs when they are within 3000 km s^{-1} of lower luminosity QSOs, but it is consistent with an inverse relationship between QSO luminosity and PDLA metallicity. One caveat is that although the N(H I) distributions are consistent between the low and high luminosity sample, the mean absorption redshift of the high luminosity sample is Δz = 0.5 higher than the low luminosity sample. Dessauges-Zavadsky et al. (2009) found that [Fe/H] changes by 0.1 dex over a Δz=0.5, whereas the logarithmic difference in metallicites inferred from the SiII EWs is 0.2 dex. Given the uncertainty of converting SiII EW to metallicity, it is premature to conclude that there is a definite link between QSO luminosity and PDLA metallicity. However, the concept of interplay between an AGN and nearby

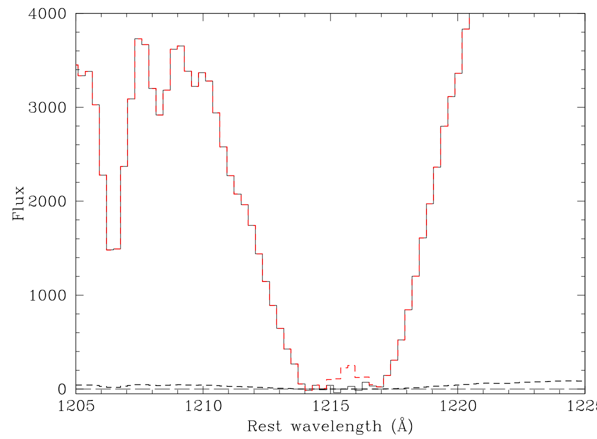

Figure 8. A zoom of the Lyα absorption trough of the stacked spectrum (black solid line) of the 29 $\Delta V \leqslant 3000$ km s^{-1} PDLAs. The red dashed line shows a simulated stack where each of the 29 PDLAs has an emission line corresponding to $L_{Ly\alpha} = 3 \times 10^{42}$ ergs/s superimposed at the centre of the Lyα absorption trough.

galactic ISM is not without precedent, either observationally or theoretically. Irwin et al. (1987) found that the radio jet axis of a nearby active galaxy was aligned with an HI tail in a close companion. They suggested that the companion's HI gas was being ram-pressure stripped by the AGN jet. Alignment of the QSO outflow with the line-of-sight has been previously invoked to explain the higher incidence of transverse DLAs, relative to the proximate line of sight absorbers (Hennawi & Prochaska 2007). In a case study of one transverse absorber located only ~ 100 kpc from the QSO, Prochaska & Hennawi (2009) find extreme kinematics and consider the case for QSO-absorber interactions. The effect of HI stripping has been modelled by Fujita (2008) and confirmed as an effective mechanism for sufficiently high energy AGN. Such interactions could prematurely (or temporarily) shut-down the star formation leading to lower metallicities. Such a scenario might also explain why the lower N(H I) PDLAs have metallicities as low as the intervening population (e.g. Table 2, Ellison et al. 2010) whereas the high N(H I) have been able to retain their gas and accrue their metals.

4.4 Lyα emission in the DLA trough

The detection of Lyα emission superimposed on the DLA trough is a rare occurence, but one that is apparently more common in PDLAs than DLAs (Møller & Warren 1993; Møller, Warren & Fynbo 1998; Leibundgut & Robertson 1999; Hennawi et al. 2009). The luminosities associated with the Lyα emission are typically 5–20 $\times 10^{42}$ ergs/s and may show large velocity widths and spatial extents of tens of kpc (Fynbo et al. 1999; Hennawi et al. 2009).

One of the PDLAs in our sample has been recently identified by Hennawi et al. (2009) as one of the most luminous PDLA Lyα emitters with a total Lyα luminosity of ~ 4×10^{43} ergs/s. Visual inspection of the rest of our sample (Figure A1) yields no other candidate Lyα emitter and there is no emission signal in the core of the composite spectrum. In order to determine an approximate limit for the emission luminosity in our combined spectrum we artifically superimpose a gaussian emission line in the core of the PDLA trough in the observed SDSS spectrum for the 29 absorbers within 3000 km s^{-1} of the QSO. The same Lyα luminosity is assumed for every PDLA, where the total integrated flux then depends only on

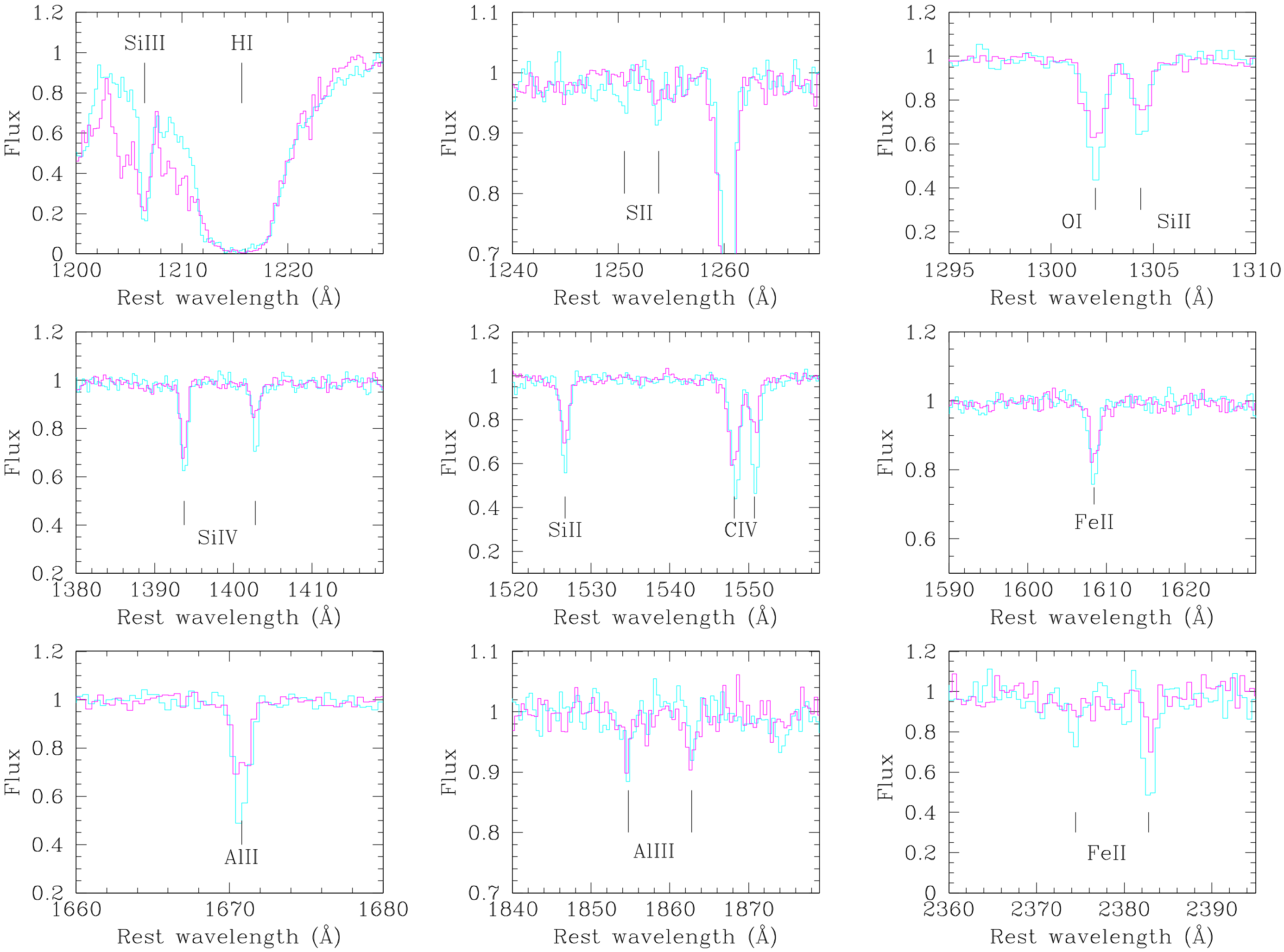

Figure 7. Median-combined composite spectrum of proximate absorbers with ΔV: < 3000 km s^{-1}, split by QSO luminosity at λ = 1500 Å. The half with the highest luminosities ($L_{1500} > 4 \times 10^{43}$ ergs/s/Å) are plotted in magenta and the half with the lowest luminosities ($L_{1500} < 4 \times 10^{43}$ ergs/s/Å) are plotted in cyan. The panels show the strongest absorption features visible in the full composite shown in Figure 2. These are the same transitions shown in Figure 3.

the luminosity distance to the absorber. The width of the emission line is set to σ= 100 km s^{-1} in all cases. The spectra are then shifted to the rest-frame with a (1+z)^4 scaling to conserve the total flux and stacked to produce a new composite. Figure 8 shows the stacked spectrum of both the original 29 low ΔV PDLAs and an overlay of one of our simulated spectra with emission (in this case where the flux corresponds to a Lyα luminosity of $L_{Ly\alpha} = 3 \times 10^{42}$ ers/s). Our tests demonstrate that the composite spectrum is sufficient to detect luminosities of a few $\times\ 10^{42}$ ergs/s if such luminosities are commonplace in PDLAs. However, this limit is likely to be optimistic for 2 reasons. First, in previous detections of Lyα emission, the emission line often appears to be offset by a few hundred km s^{-1} from the centre of the Lyα absorption trough. Stacking analyses are quite sensitive to such offsets (Ellison et al. 2000). Second, if the flux is spread out over many hundreds of km s^{-1}, as seen by Hennawi et al. (2009), the broader profile becomes more difficult to detect. In the absence of a well characterized distribution of line offsets and widths, it would be premature to attempt more sophisticated stacking simulations.

5 DUST IN PDLAS

Over the past two decades, there has been considerable debate in the literature regarding the amount of dust extinction associated with DLAs. Although these studies may disagree in the details, there is now a broad concensus in the contemporary literature that the typical dust reddening is small. Some examples of recent works on this topic and detections or limits on the reddening include Murphy & Liske (2004) [E(B−V) < 0.01], Ellison, Hall & Lira (2005) [E(B−V) < 0.04], Vladilo et al. (2008) [E(B−V) = 0.006] and Frank & Peroux (2010) who find a best fit E(B−V) = −0.002, i.e. consistent with no reddening.

In this section, we investigate whether the PDLAs have extinction properties that are consistent with the intervening population, since there are several *a priori* reasons to expect that they may differ. As we have demonstrated above, the PDLAs (particularly those at low ΔV with high N(H I)) have higher metallicities, which appear to go hand-in-hand with higher gas phase depletion indicators (e.g. Prochaska & Wolfe 2002). Moreover, Kaplan et al. (2010) have shown that their sample of metal-strong DLAs (a sample which overlaps considerably with our PDLAs, as we discuss in the next section) have systematically redder spectra than a sample of control (non-metal strong) DLAs. Finally, proximate MgII absorbers at $z \sim$ 1–2 have reddening values that are approximately twice that of the intervening MgII systems: E(B−V) = 0.02 and 0.01 respectively (Vanden Berk et al. 2008; York et al. 2006).

There are three main techniques for determining the reddening in a sample of DLAs. The first uses broad band colour information, usually in the optical (e.g. Khare et al. 2004; Vladilo et al. 2006, 2008), but if IR photometry is also available, a more stringent limit can be obtained (e.g. Ellison et al. 2005). If spectral data are available, a more detailed extinction analysis is possible and there are two main techniques that have been applied. The first involves fitting a power law to unabsorbed regions of the QSO continuum, avoiding the emission features (e.g. Pei, Fall & Bechtold 1991; Murphy & Liske 2004; Kaplan et al. 2010). The second involves making composite spectra of an absorber and non-absorber sample, where the ratio reveals the average extinction curve of the former (e.g. York et al. 2006; Wild et al. 2006; Vanden Berk et al. 2008; Frank & Peroux 2010). We have experimented with both techniques. The composite method was found to be fundamentally limited (in our relatively small sample) by our ability to average out the range of underlying QSO properties. Although this technique has been used successfully on smaller samples than ours (e.g. Wild et al. 2006), the redshift range of our absorbers is such that there are many emission lines in our rest-frame spectrum. As noted by Frank & Peroux (2010), this leads to residuals and structure in the region 1300-1700 Å. Despite various attempts at matching parameters, we were unable to overcome this limitation and were always dominated by the underlying variation in emission line properties. This may be mitigated in larger samples (e.g. Frank & Peroux 2010) where residuals lead to an apparent bluing of only E(B−V)~ -0.002.

Instead, we adopted the approach of fitting emission- and absorption-free regions of the QSO continua with a power law and examining the difference in spectral indices of the PDLAs and a control sample of no-PDLA QSOs. The technique is the same as we have applied previously in Kaplan et al. (2010). In brief, the median flux of up to seven emission-free regions (1312–1328, 1345–1365, 1430–1475, 1680–1700, 2020–2040, 2150–2170, and 2190–2250 Å) is calculated from the rest-frame QSO spectrum. The number of regions depends on the QSO redshift: Higher redshift QSOs will have few spectral regions to fit, as the redder regions are shifted beyond the SDSS spectral coverage. A power law of the form $f(\lambda) \propto \lambda^{-\alpha}$ is fit to these median values where reddening due to dust will lead to smaller values of α. An example of the fitting procedure is shown in Figure 9. Three QSOs have 2 PDLAs in their line of sight. These were excluded from the analysis, leaving a sample of 79 PDLAs. Fitting is also performed for the 20 control QSOs (Section 2.2) matched to each of the 79 PDLAs (i.e. a total of 1580 control spectra). The use of control spectra matched in redshift and magnitude will help circumvent any bias from the dependence of continuum slope on luminosity or the number of wavelength windows fitted. We have additionally checked that there is no overall trend of α with redshift in the control sample.

The top panel of Figure 10 shows the fractional distribution

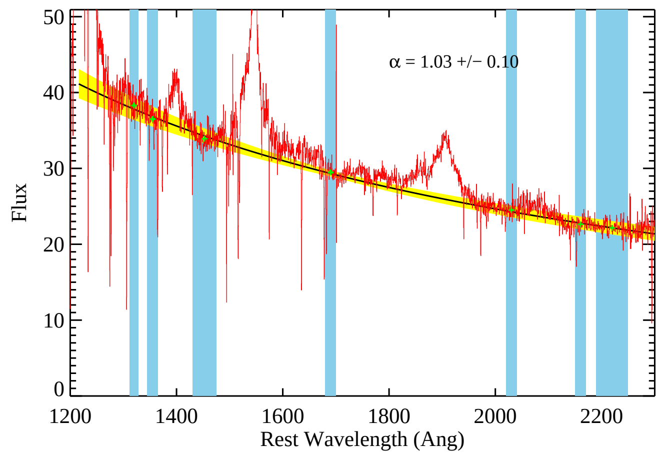

Figure 9. Example of the spectral fitting procedure. A power law ($f(\lambda) \propto \lambda^{-\alpha}$) fit is made to the median value (small green crosses) in each of up to seven continuum regions (vertical blue shaded bands). The solid black line shows the fit and the yellow region shows the uncertainty as a function of rest-frame wavelength.

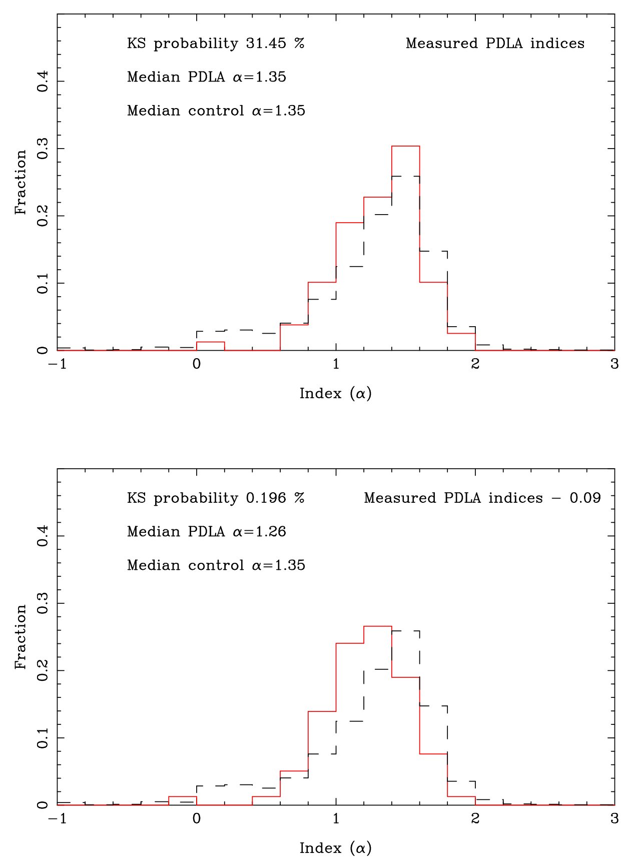

Figure 10. Fractional distribution of power law indices for the PDLA sample (red solid histogram) and matched control QSO sample (black dashed histogram). There are 20 control QSOs for every QSO with a PDLA. The upper panel shows the distribution of measured PDLA indices. The lower panel shows the PDLA indices decreased by a value of 0.09 which is the offset required to yield a KS value less than 0.3 % (3 σ rejection of the null hypothesis). The control histrogram is the same in both panels.

of power law indices in the PDLA and control sample. A KS test indicates that there is no statistical difference between the distributions and the two samples have the same median value. In order to determine a limit for the reddening in our sample, we estimate the minimum change in the indices of the PDLA sample that would have resulted in a KS test probability of 0.3% that it is drawn from the same distribution as the control (corresponding to a 3 σ certainty). Small incremental increases are made to the observed indices of the QSOs with PDLAs and the KS probability (relative to the control) is re-computed until the value reaches 0.3%. Considering all 79 PDLAs, decreasing all the indices by a single value of 0.09 yields a KS probability below 0.3%. The new distribution of PDLA indices is shown in the lower panel of Figure 10.

The sample of 79 PDLAs includes absorbers with ΔV values as large as 10,000 km s^{-1}. At such large velocity separations the absorbers are likely to be dominated by the intervening population. However, we find that comparing only the lower ΔV subsamples with their control still yields no significant difference in the distribution of α. There is also no difference in the continuum slopes when the sample is split by N(H I). We repeat the above procedure for determining the minimum difference in α that would result in a significant KS result. For the $\Delta V < 6000$ km s^{-1} absorbers (51 PDLAs) we again find an index decrease of 0.09 before the KS probability drops below 0.3%. For the $\Delta V < 3000$ km s^{-1} (28 absorbers) the test is less sensitive and an index change of 0.19 is required before the distribution is significantly different from the control. Using the smaller data set therefore provides the more stringent constraint on reddening.

To convert the index change that results in a significant KS probability into a measure of dust extinction, we define the difference between the control and PDLA indices as $\delta\alpha = \alpha_c - \alpha_P$. As described in Kaplan et al. (2010), we can write the colour excess at two wavelengths as a function of $\delta\alpha$:

$$E_{\lambda_1-\lambda_2} = -2.5.log_{10}\left[\left(\frac{\lambda_1}{\lambda_2}\right)^{\delta\alpha}\right]. \quad (1)$$

The values of λ_1 and λ_2 are set to be 1300 and 2000 Å respectively, as values that are typical of the coverage of our spectra. In order to convert this colour excess at λ_1 and λ_2 into the more standard notation of E($B-V$), we adopt the SMC extinction curve of Pei (1992). We define $\xi(\lambda) = A_\lambda/A_V$, so that[1]

$$E_{\lambda_1-\lambda_2} = A_{\lambda_1} - A_{\lambda_2} = A_V(\xi_{\lambda_1} - \xi_{\lambda_2}). \quad (2)$$

Combining these equations for a $\delta\alpha = 0.09$ and 0.19 we derive an $A_V = 0.020$ and 0.041 respectively. To convert to an E($B-V$) we use the standard definition $R_V = A_V/E(B-V)$ with $R_V = 2.93$. For a $\delta\alpha = 0.09$ and 0.19 we arrive at upper limits to the colour excesses of E($B-V$) = 0.007 (ΔV< 10,000 km s^{-1} and ΔV< 6000 km s^{-1} samples) and 0.014 (ΔV< 3000 km s^{-1} sample) respectively.

An alternative technique for identifying differences in the PDLA and control sample is to calculate the difference between the α of the PDLA spectrum and the mean of its 20 control galaxies. These 'α offsets' are plotted as a function of ΔV in Figure 11 and should be zero if the QSO with the PDLA has a continuum slope that is the same as the mean of its controls. Negative values of the α offset indicate that the PDLAs are redder than their controls, on average. Figure 11 appears to show that QSOs with PDLAs whose $\Delta V < 2000$ km s^{-1} are *bluer* than their matched controls. At larger ΔV there is no significant ($> 3\sigma$) offset. Even though we take the median flux in the continuum windows to account for the effect of absorption features, one may be concerned that indices may be biased in certain velocity intervals as strong absorption lines move through. In order to make the PDLA spectrum bluer, additional absorption at the red end of the spectrum would be required. A review of Figure 2 shows that the only strong lines beyond 1700 Å are the FeII lines at $\lambda_0 > 2300$ Å and are therefore too red to ever enter any of our continuum windows. Intrinsic dependences of the index on QSO redshift and magnitude are accounted for in the matching procedure. Drawing samples at random from the full α offset distribution indicates that the positive offset seen at $\Delta V < 2000$ km s^{-1} would be expected 5% of the time for bins of this size. Larger samples are therefore required to determine whether this result is due to small number statistics.

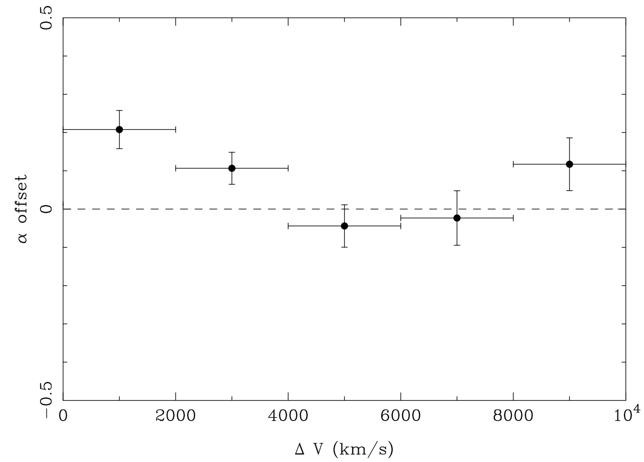

Figure 11. α offset is defined as the index of the PDLA QSO spectrum minus the mean value of the index of its 20 control QSOs. The mean α offset and 1σ error bars are plotted in bins of ΔV. Based on a random sampling of the full α offset distribution, the high value seen in the $\Delta V < 2000$ km s^{-1} bin has a 5% chance of occurring by chance in a sample of this size.

6 DISCUSSION

A similar analysis to the one presented here has been performed for 415 proximate MgII absorbers (EW > 0.3 Å) within $\Delta V < 3000$ km s^{-1} of the QSO by Vanden Berk et al. (2008). They find that the low ionization lines (MgII and AlII) have similar equivalent widths in the proximate and intervening composites, whereas the high ionization lines (CIV and SiIV) are stronger in the $\Delta V < 3000$ km s^{-1} sample. Vanden Berk et al (2008) conclude that this is caused by higher ionization in the proximate MgII systems. Although we also find that the CIV and SiIV EWs are 2–3 larger in the PDLAs at $\Delta V < 3000$ km s^{-1}, compared to the $\Delta V > 6000$ km s^{-1} sample, the low ionization lines such as SiII and FeII are also up to a factor of 2 stronger. The relative strengths of low and high ionization lines is probably related to the N(H I) of the sample. The MgII absorbers in Vanden Berk et al. (2008) are likely to have H I column densities that extend down to log N(H I) ~ 17.5. Their composites will therefore be skewed towards lower N(H I) values than ours. When we consider the lower half of our N(H I) distribution (log N(H I) < 20.7) we also find that the EWs of the low ions become more consistent in the low and high ΔV samples (Figures 4 and 5). The clearest distinction in the metallicities of $\Delta V < 3000$ km s^{-1} relative to larger velocity separations is also seen when the N(H I) is large

[1] Pei (1992) defines $\xi(\lambda) = A_\lambda/A_B$, so we have included a factor of 1.33 to the values of ξ derived from the Pei extinction curve.

(see also Ellison et al. 2010). This may again explain why Vanden Berk et al. (2008) did not find evidence for enhanced metallicities in their proximate MgII sample, whereas our PDLAs show systematically larger low ionization metal line EWs at small ΔV.

Figure 3 and Table 2 show that the majority of the transitions in the $3000 < \Delta V < 6000$ km s^{-1} composite exhibit EWs that are intermediate between the low and high velocity composites. This indicates that the 3000 – 6000 km s^{-1} absorbers may not yet have reached the same typical values as intervening absorbers. We can attempt to achieve some finer ΔV resolution by utilizing the SiII λ 1526 line which is detected in 72/85 of the individual SDSS PDLA spectra. In cases of a non-detection, the rest-frame 3 σ limit was calculated from the rest-frame spectrum using the equation $3\sigma = \frac{3 \times FWHM}{S/N}$. The FWHM at 1526 Å is taken to be 0.85 Å (based on the nominal SDSS resolution of $R = \lambda/\Delta\lambda = 1800$). The EW of this (usually saturated) SiII line correlates with metallicity (Prochaska et al. 2008a) so can be used as an approximate metallicity metric. In Figure 12 we show the median SiII λ 1526 EW in bins of ΔV (middle panel) and the corresponding metallicity calibrated by the Prochaska et al. (2008a) relation (bottom panel). The enhanced metallicity is seen most convincingly in the lowest velocity bin ($\Delta V < 0$ km s^{-1}) and is due to a combination of a lack of low EWs, as well as values that range up to 1 Å in equivalent width. The results earlier in this paper would further lead us to expect that this will depend on the N(H I) of the individual absorbers, but we do not have the numbers to test both the ΔV and N(H I) distributions separately in this way.

Although the median SiII EW is only enhanced at $\Delta V < 0$ km s^{-1}, Figure 12 shows a notable population of high EW SiII absorbers at larger velocity separations, particularly around $3000 < \Delta V < 5000$ km s^{-1}. These are likely to be the absorbers that lead to the generally larger EWs measured in the intermediate velocity composite ($3000 < \Delta V < 6000$ km s^{-1}). Although SiII EW is not a very accurate estimator of metallicity, the detection of SiII λ 1808 (with EWs> 150 mÅ) in approximately half of the $3000 < \Delta V < 5000$ km s^{-1} PDLAs with SiII EW > 900 mÅ is strongly suggestive of high metallicities. It may be surprising that QSO proximity is responsible for enhanced metallicities at $\Delta V > 3000$ km s^{-1} (which corresponds to a Hubble flow distance of $\sim$ 10 proper Mpc at $z = 3$). Although the redshifts derived from the SDSS spectra by PHHF08 are improved from those determined from Lyα and CIV emission lines alone, they are likely still only *statistically* accurate to within a few hundred km s^{-1} (Shen et al. 2007). However, the presence of a population of PDLAs with $-2000 < \Delta V < 0$ indicates that a combination of non-Hubble flow velocities and redshift errors can account of $\sim$ 2000 km s^{-1} in velocity range. Individual IR spectra of these QSOs are required in order to determine accurate relative velocities. The uncertain nature of these intermediate ΔV absorbers means that, even with a sample of 85 SDSS spectra, it is not possible to determine what the correct cut-off should be for studies that aim to sample the truly intervening population. Our results indicate that the largest effect occurs at velocities well below the cut-offs typically used in DLAs surveys ($\sim$ 3000 km s^{-1}). However, a more conservative approach (until a larger statistical study can be undertaken) would be to increase the ΔV cut-off from 3000 to 6000 km s^{-1}.

Although the majority of DLAs are metal-poor, a few rare examples of high metallicities have been reported in the literature, although mostly in the lower N(H I) sub-DLAs (e.g. Prochaska et al. 2006; Peroux et al. 2008; Meiring et al. 2008; Dessauges-Zavadsky, Ellison & Murphy 2009). The very large samples of QSOs assembled by the SDSS has also permitted the identification of unusually high metallicity systems. Herbert-Fort et al. (2006) identified absorbers with large metal line equivalent widths from the SDSS DR3 spectra. These metal-strong (MS) DLAs are of particular interest for detecting rare elements, such as boron, germanium and cobalt (Ellison, Ryan & Prochaska 2001; Prochaska et al. 2003). It is estimated that this metal-strong population represents only $\sim$ 5% of the DLA population. Kaplan et al. (2010) have determined abundances for a sample of 16 MS DLAs finding a median metallicity $Z \sim 1/5 Z_\odot$ at $z \sim 2$, a factor of around 4 higher than their control sample of non-MS DLAs. We have compared our sample of 85 PDLAs (Table 1) to the list of MS DLAs in Herbert-Fort et al. (2006). 11 PDLAs (13%) are present in the compilation of Herbert-Fort et al. (2006), see Table 3. However, only 45/85 of the QSOs in Table 1 were present in the DR3 (recall that our sample is drawn from the DR5). Therefore, whereas only $\sim$ 5% of intervening DLAs are metal-strong, the percentage rises to 11/45=24% for PDLAs.

One of the PDLAs in our sample is the proto-typical MS DLA

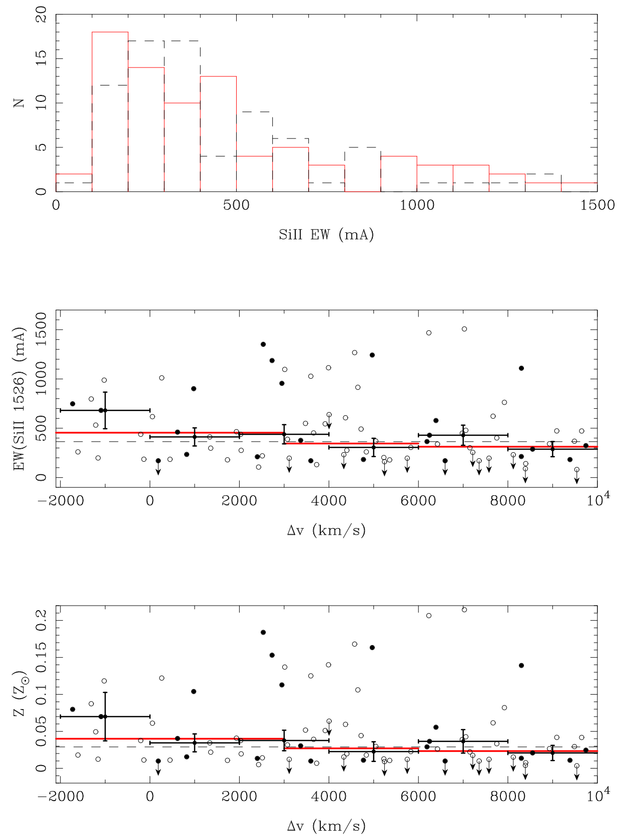

Figure 12. Top panel: Distribution of SiII λ 1526 EWs for the PDLAs (solid red line) and matched control sample of intervening DLAs (dashed black line). Middle panel: Rest-frame EWs of the SiII λ 1526 line as a function of velocity offset from the QSO. Limits are 3σ. The open circles show individual PDLA measurements and the solid circles are median values in velocity bins of width 2000 km s^{-1}. The median is selected so that the small number of SiII upper limits can be considered as detections without affecting the binned value. The horizontal dashed line is the median value of SiII λ 1526 EWs of the intervening control sample. Lower panel: SiII λ 1526 EWs have been converted to metallicities (relative to the Sun) using the calibration of Prochaska et al. (2008a): $\log Z/Z_\odot = 1.41 \log(W) - 0.92$, where W is the SiII EW in Å. The horizontal dashed line is the median metallicity calculated from the SiII λ 1526 EWs of the intervening control sample. Errors are 1σ.

QSO	z_{em}	z_{abs}	log N(H I)	ΔV (km s^{-1})
J075901.28+284703.4	2.8550	2.8223	21.05	2532.00
J081240.68+320808.6	2.7045	2.6259	21.30	6391.40
J095817.81+494618.3	2.3555	2.2909	20.65	5831.18
J101725.88+611627.5	2.8069	2.7681	20.60	3073.19
J102619.09+613628.8	3.8442	3.7853	20.35	3657.30
J113008.19+535419.8	3.0495	2.9870	20.25	4575.67
J122040.23+092326.8	3.1462	3.1322	20.75	978.39
J135305.18-025018.2	2.4149	2.3618	20.30	4647.59
J160413.97+395121.9	3.1542	3.1625	21.75	-656.45
J210025.03-064146.0	3.1295	3.0918	21.05	2729.34
J232115.48+142131.5	2.5539	2.5729	20.60	-1607.98

Table 3. PDLAs identified as 'metal-strong' in the DR3 catalogue of Herbert-Fort et al. (2006).

J081240.6+320808[2]. In a case study of this absorber, Prochaska et al. (2003) used data obtained with HIRES to make the first detections of several elements never before detected outside the local group. J081240.6+320808 is notable because it shows SiII λ 1808 (EW ~ 260 mÅ) absorption even in the SDSS spectrum. As described above, SiII λ 1808 is observed in several of the individual SDSS spectra, including J075901+284703, J113008+535419, J135305−025018, J160413.97+395121 and J210025.03-064146 which appear in the MS DLA catalogue of Herbert-Fort et al. (2006). To demonstrate the large EWs of these metal-strong PDLAs, in Figure 13 we show the SDSS spectrum of J160413.97+395121 compared with that of J081240.6+320808. J160413.97+395121 has been subsequently studied at high resolution by Ellison et al. (2010), who confirm a relatively high metallicity ~ 1/16 $Z_\odot$. J210025.03-064146.0 was observed with ESI by Herbert-Fort et al. (2006) and measured to have an even higher metallicity: Z ~ 1/5 $Z_\odot$.

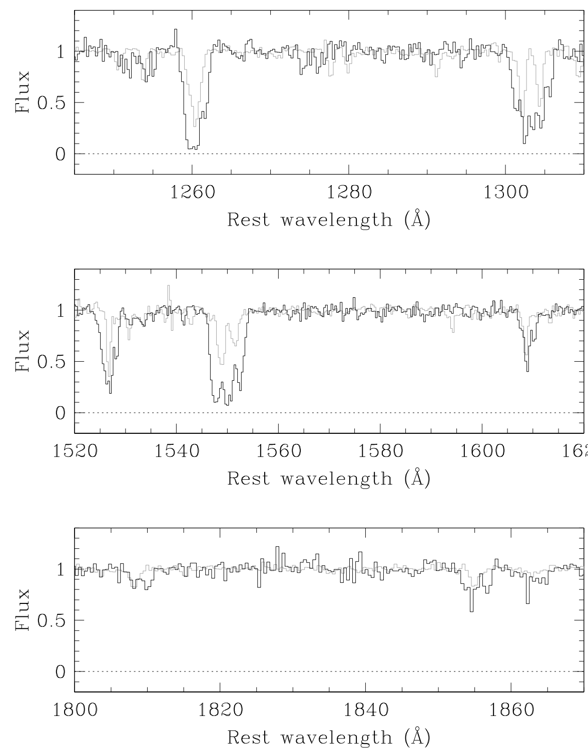

Figure 13. Selected regions of the SDSS spectrum of J160413.97+395121.9 (black) with the SDSS spectrum of the prototypical metal-strong DLA J081240.68+320808.6 (grey) overlaid. The top panel includes detections of SII $\lambda\lambda$ 1250, 1259, SiII λ 1260, OI λ 1302 and SiII λ 1304. The middle panel includes detections of SiII λ1526, CIV $\lambda\lambda$ 1548, 1550 and FeII λ 1608. The lower panel covers SiII λ 1808 and Al III $\lambda\lambda$ 1854, 1862.

Although the PDLAs and MS DLAs may both preferentially sample the high metallicity end of the DLA distribution, they differ markedly in their extinction properties. Whereas the general DLA population causes very little reddening to the background QSO (Murphy & Liske 2004; Ellison et al. 2005; Vladilo et al. 2008; Frank & Peroux 2010), Kaplan et al (2010) find significantly flatter power law slopes in QSOs behind MS DLAs. Using the methodology described in Section 5 and adopting our choice of SMC extinction curve and R_V, their report value of $\delta\alpha$ = 0.29 corresponds to A_V = 0.063 and E($B - V$) = 0.022. In contrast, our most stringent limit (derived for the ΔV < 3000 km s^{-1} sample) gives A_V < 0.041 and E($B - V$) < 0.014 for the PDLAs. The reddening by PDLAs is also less than for associated MgII systems at z ~ 1–2 [E(B−V) = 0.02, Vanden Berk et al. 2008], although this may be at least in part due to the redshift evolution of reddening in MgII absorbers (Menard et al. 2008). However, our detection limit is not sufficiently sensitive to determine whether or not the PDLAs are more or less dusty than their intervening cousins.

We have presented evidence in this paper and in Ellison et al. (2010) that some PDLAs (those with small ΔV and large N(H I)) appear more metal-rich than the intervening population. However, the sample of PDLAs in Ellison et al. (2010) includes an absorber with one of the lowest metallicities measured to date (J0140−0839, [O/H]=−2.72). In Section 4.3 we have shown that for PDLAs with ΔV < 3000 km s^{-1}, the composite SDSS spectra show weaker metal lines when the QSO luminosity is higher. J0140−0839 (ΔV= 1250 km s^{-1}) is included in the PDLA sample of PHHF08, but excluded by us because the QSO shows mild BAL features. Nonetheless it is intriguing that J0140−0839 has a relatively large luminosity: L_{1500} = 1.3 × 10^{44} ergs/s/Å, a value exceeded by only two of the QSOs in our sample. There are 4 QSOs in our sample with L_{1500} > 1 × 10^{44} ergs/s/Å: J082638.59+515233.2, J090033.49+421546.8, J092914.49+282529.1 and J095937.11+131215.4). The latter two have very large relative velocities from the QSO (ΔV > 9500 km s^{-1}). We inspected the metal lines of J082638.59+515233.2, J090033.49+421546.8 (ΔV = 820 and 3477 km s^{-1} respectively) in the SDSS spectra and did not find them to be abnormally low. High luminosities and moderate relative velocities do therefore not necessarily lead to low metallicities.

7 SUMMARY

We have used a sample of 85 proximate absorbers in the SDSS with ΔV < 10,000 km s^{-1} and log N(H I) ⩾ 20 to investigate trends of metal line strength with velocity separation. Composite spectra

[2] We emphasize again that for convenience, in this paper we are using the term 'PDLA' for absorbers with log N(H I) > 20 and ΔV < 10,000 km s^{-1}, which is the range over which we look for trends. A stricter definition would adopt the standard DLA criterion of log N(H I) ⩾ 20.3. Moreover, at large ΔV our sample will include an increasing fraction of intervening absorbers.

are constructed for 3 ΔV ranges: $\Delta V < 3000$ km s^{-1}, $3000 < \Delta V < 6000$ km s^{-1} and $\Delta V > 6000$ km s^{-1}. The samples are further divided according to H I column density and QSO luminosity. Our main findings are as follows:

(i) Metal line EWs are largest in the $\Delta V < 3000$ km s^{-1} composite and smallest at $\Delta V > 6000$ km s^{-1}. At intermediate velocities ($3000 < \Delta V < 6000$ km s^{-1}) the EWs are between the low and high ΔV composites. We interpret this result as caused by higher metallicities at lower relative velocities.

(ii) Although the intermediate velocity composite indicates that enhanced metallicities might exist out to several thousands of km s^{-1} from the systemic QSO redshift, measurements of SiII λ 1526 in individual spectra indicate that the metallicity is most enhanced at $\Delta V < 0$ km s^{-1}.

(iii) The difference between the EWs in the lowest ($\Delta V < 3000$ km s^{-1}) and highest ($\Delta V > 6000$ km s^{-1}) composites is largest when only the high N(H I) (log N(H I) $\geqslant 20.7$) are considered. Using the SiII λ 1526 EW-metallicity relation of Prochaska et al. (2008a), we determine metallicities of 1/12 and 1/45 for the low and high ΔV composites respectively, when N(H I) $\geqslant$ 20.7.

(iv) The absorbers within 3000 km s^{-1} of high luminosity QSOs have lower metal line EWs than those within 3000 km s^{-1} of low luminosity QSOs. We speculate that this may be due to truncation of star formation in the vicinity of a more luminous AGN. However, a low ΔV and high QSO luminosity does not necessarily lead to lower EWs.

(v) Using the classifications of Herbert-Fort et al. (2006) we have also shown that PDLAs are 5 times more likely to be 'metal-strong' than intervening DLAs. We present 4 PDLAs whose SiII λ 1808 is strong enough to be be detected even in the SDSS spectra which are also classified as MSDLAs, making them excellent candidates for follow-up of rare species.

(vi) No Lyα emission is detected in the PDLA trough of the composite. Although an accurate flux limit is difficult to model based on the uncertainty of line emission properties, our simulations indicate that typical Lyα luminosities of a few $\times 10^{42}$ would have been detected.

(vii) From an analysis of the power law slopes of QSOs with PDLAs compared to a matched control sample, we place an upper limit of E($B-V$) < 0.014 (for an SMC extinction curve) on the reddening caused by PDLAs. This is less than inferred from a similar analysis of MS DLAs, and a complementary investigation of reddening in proximate MgII absorbers at $z \sim 1.5$.

Our findings are consistent with measurements in a smaller sample (16 PDLAs) of high resolution spectra which find that high N(H I) PDLAs are more metal-rich than the intervening population by a factor of ~ 3 (Ellison et al. 2010). Taken together, these results are evidence that galaxies in the vicinity of QSOs not only differ from the intervening population but are directly affected by the proximity of a QSO.

ACKNOWLEDGMENTS

SLE acknowledges support from an NSERC Discovery Grant and Discovery Accelerator Supplement. Thank you to Andrew Fox for useful suggestions on an earlier draft of this paper.

Funding for the SDSS and SDSS-II has been provided by the Alfred P. Sloan Foundation, the Participating Institutions, the National Science Foundation, the U.S. Department of Energy, the National Aeronautics and Space Administration, the Japanese Monbukagakusho, the Max Planck Society, and the Higher Education Funding Council for England. The SDSS Web Site is http://www.sdss.org/.

The SDSS is managed by the Astrophysical Research Consortium for the Participating Institutions. The Participating Institutions are the American Museum of Natural History, Astrophysical Institute Potsdam, University of Basel, University of Cambridge, Case Western Reserve University, University of Chicago, Drexel University, Fermilab, the Institute for Advanced Study, the Japan Participation Group, Johns Hopkins University, the Joint Institute for Nuclear Astrophysics, the Kavli Institute for Particle Astrophysics and Cosmology, the Korean Scientist Group, the Chinese Academy of Sciences (LAMOST), Los Alamos National Laboratory, the Max-Planck-Institute for Astronomy (MPIA), the Max-Planck-Institute for Astrophysics (MPA), New Mexico State University, Ohio State University, University of Pittsburgh, University of Portsmouth, Princeton University, the United States Naval Observatory, and the University of Washington.

REFERENCES

Dessauges-Zavadsky, M., Calura, F., Prochaska, J. X., D'Odorico, S., Matteucci, F., 2004, A&A, 416, 79
Dessauges-Zavadsky, M., Prochaska, J. X., D'Odorico, S., Calura, F., Matteucci, F., 2006, A&A, 445, 93
Dessauges-Zavadsky, M., Ellison, S. L., Murphy, M. T., 2009 MNRAS, 396, L61
Ellison, S. L., 2006, MNRAS, 368, 335
Ellison, S. L., Hall, P. B., Lira, P., 2005, AJ, 130, 1345
Ellison, S. L., Murphy, M. T., Dessauges-Zavadsky, M., 2009, MNRAS, 392, 998
Ellison S. L., Prochaska, J. X., Hennawi, J., Lopez, S., Usher, C. G., Wolfe, A. M., Russell, D., Benn, C. R., MNRAS, 2010, 406, 1435
Ellison, S. L., Ryan, S. & Prochaska, J. X., 2001, MNRAS, 326, 628
Ellison, S. L., Songaila, A., Schaye, J., Pettini, M., 2000 AJ, 120, 1175
Ellison, S. L., Yan, L., Hook, I., Pettini, M., Wall, J., Shaver, P., 2001, A&A, 379, 393
Ellison, S. L., Yan, L., Hook, I., Pettini, M., Wall, J., Shaver, P., 2002, A&A, 383, 91
Ellison, S. L., York, B. A., Pettini, M., Kanekar, N., 2008, MNRAS, 388, 1349
Fox, A. J., Ledoux, C., Petitjean, P., Srianand, R., 2007a, A&A, 473, 791
Fox, A. J., Petitjean, P., Ledoux, C., Srianand, R., 2007b, A&A, 465, 171
Fox, A. J., Prochaska, J. X., Ledoux, C., Petitjean, P., Wolfe, A. M., Srianand, R., 2009, A&A, 503, 731
Frank, S., & Peroux, C., 2010, MNRAS, 406, 2235
Fujita, Y., 2008, MNRAS, 384, L41
Fynbo, J. U., Burud, I., Møller, P., 2000, A&A, 358, 88
Fynbo, J. U., Møller, P., Warren, S. J., 1999, MNRAS, 305, 849
Gaskell, C. M., 1982, ApJ, 263, 79
Hennawi, J. F., & Prochaska, J. X., 2007, ApJ, 655, 735
Hennawi, J. F., Prochaska, J. X., Kollmeier, J., Zheng, Z., 2009, ApJ, 693, L49
Herbert-Fort, S., Prochaska, J. X., Dessauges-Zavadsky, M., Ellison, S. L., Howk, J. C., Wolfe, A. M., Prochter, G. E., 2006, PASP, 118, 1077
Howk, J.C., & Sembach, K.R. 1999, ApJ, 523, L141
Irwin, J. A., Seaquist, E. R., Taylor, A. R., Duric, N., 1987, ApJ, 313, L91
Jorgenson, R., Wolfe, A. M., Prochaska, J. X., Lu, L., Howk, J. C., Cooke, J., Gawiser, E., Gelino, D., 2006, ApJ, 646, 730
Kaplan, K. F., J. X., Prochaska, Herbert-Fort, S., Ellison, S. L., Dessauges-Zavadsky, M., 2010, PASP, 122, 619
Khare, P., Kulkarni, V. P., Lauroesch, J. T., York, D. G., Crotts, A. P. S., Nakamura, O., 2004, ApJ, 616, 86
Krumholz, Ellison, S. L., Prochaska, J. X., Tumlinson, J., 2009, ApJ, 701, L12
Lanzetta, K. M., McMahon, R. G., Wolfe, A. M., Turnshek, D. A., Hazard, C., & Lu, L. 1991, ApJS, 77, 1
Lanzetta, K. M., Wolfe, A. M., Turnshek, D. A., 1995, ApJ, 440,435

Ledoux, C., Petitjean, P., Fynbo, J. P. U., Moller, P., Srianand, R., 2006, A&A, 457, 71
Leibundgut, B., & Robertson, J. G., 1999, MNRAS, 303, 711
Meiring, J. D., Kulkarni, V. P., Lauroesch, J. T., Peroux, C., Khare, P., York, D. G., Crotts, A. P. S., 2008, MNRAS, 384, 1015
Menard, B., Nestor, D., Turnshek, D., Quider, A., Richards, G., Chelouche, D., Rao, S., 2008, MNRAS, 385, 1053
Milutinovic, N., Ellison, S. L., Prochaska, J. X., Tumlinson, J., 2010, MNRAS, in press
Møller, P., Warren, S. J., 1993, A&A, 270, 43
Møller, P., Warren, S. J., Fynbo, J. U., 1998, A&A 330, 19
Murphy, M. T., Curran, S. J., Webb, J. K., Menager, H., Zych, B. J., 2007, MNRAS, 376, 673
Murphy, M. T., & Liske, J., 2004, MNRAS, 345, L31
Nestor, D. B., Rao, S. M., Turnshek, D. A., Vanden Berk, D., 2003, ApJ, 595, L5
Noterdaeme, P., Petitjean, P., Ledoux, C., Srianand, R., 2009, A&A, 505, 1087
Pei, Y., 1992, ApJ, 395, 130
Pei, Y., Fall, S. M., Bechtold, J., 1991, ApJ, 378, 6
Peroux, C., Meiring, J. D., Kulkarni, V. P., Khare, P., Lauroesch, J. T., Vladilo, G., York, D. G., 2008, MNRAS, 386, 2209
Peroux, C., Storrie-Lombardi, L. J., McMahon, R. G., Irwin, M., Hook, I. M., 2001, AJ, 121, 1799
Pettini, M., Smith, L.J., Hunstead, R.W., King, D.L., 1994, ApJ, 426, 79
Prochaska, J. X., Chen, H.-W., Wolfe, A. M., Dessauges-Zavadsky, M., Bloom, J. S., 2008a, ApJ, 672, 59
Prochaska, J. X., Henry, R., O'Meara, J., Tytler, D., Wolfe, A., Kirkman, D., Lubin, D., Suzuki, N., 2002a, PASP, 114, 933
Prochaska, J. X., Hennawi, J. F., 2009, ApJ, 690, 1558
Prochaska, J. X., Hennawi, J. F., & Herbert-Fort, S., 2008b, ApJ, 675, 1002 (PHHF08)
Prochaska, J. X., Howk, J. C., O'Meara, J. M., Tytler, D., Wolfe, A. M., Kirkman, D., Lubin, D., Suzuki, N., 2002b, ApJ, 571, 693
Prochaska, J. X., Howk, J. C., Wolfe, A. M., 2003, Nature, 423, 57
Prochaska, J. X. O'Meara, J. M., Herbert-Fort, S., Burles, S., Prochter, G. E., Bernstein, R. A., 2006, ApJ, 648, L97
Prochaska, J. X., & Wolfe, A. M. 2002, ApJ, 566, 68
Prochaska, J. X., Wolfe, A. M., 2009, ApJ, 696, 1543
Rix, S. A., Pettini, M., Steidel, C. C., Reddy, N. A., Adelberger, K. L., Erb, D. K., Shapley, A. E., 2007, ApJ, 670, 15
Schaye, J., 2001, ApJL, 562, L95
Shen, Y., et al. 2007, AJ, 133, 2222
Storrie-Lombardi, L., McMahon R. G., & Irwin, M., Hazard, C., 1996, MNRAS, 468, 121
Vanden Berk, D. E., et al., 2008, ApJ, 679, 239
Vladilo, G., Centurion, M., Bonifacio, P., Howk, J. C., 2001, ApJ, 557, 1007
Vladilo, G., Centurion, M., Levshakov, S., Peroux, C., Khare, P., Kulkarni, V., York, D. G., 2006, A&A, 454, 151
Vladilo, G., Prochaska, J. X., Wolfe, A. M., 2008, A&A, 478, 701
Wild, V., Hewett, P. C., & Pettini, M., 2006, MNRAS, 367, 211
Wolfe, A. M., Lanzetta, K. M., Foltz, C. B., Chaffee, F. H., 1995, ApJ, 454, 698
York, D. G., et al. 2006, MNRAS, 367, 945

APPENDIX A: PDLAS IN THE SDSS SAMPLE

In Figure A1 we present the fits to the Lyα absorption of the 85 PDLAs in our sample.

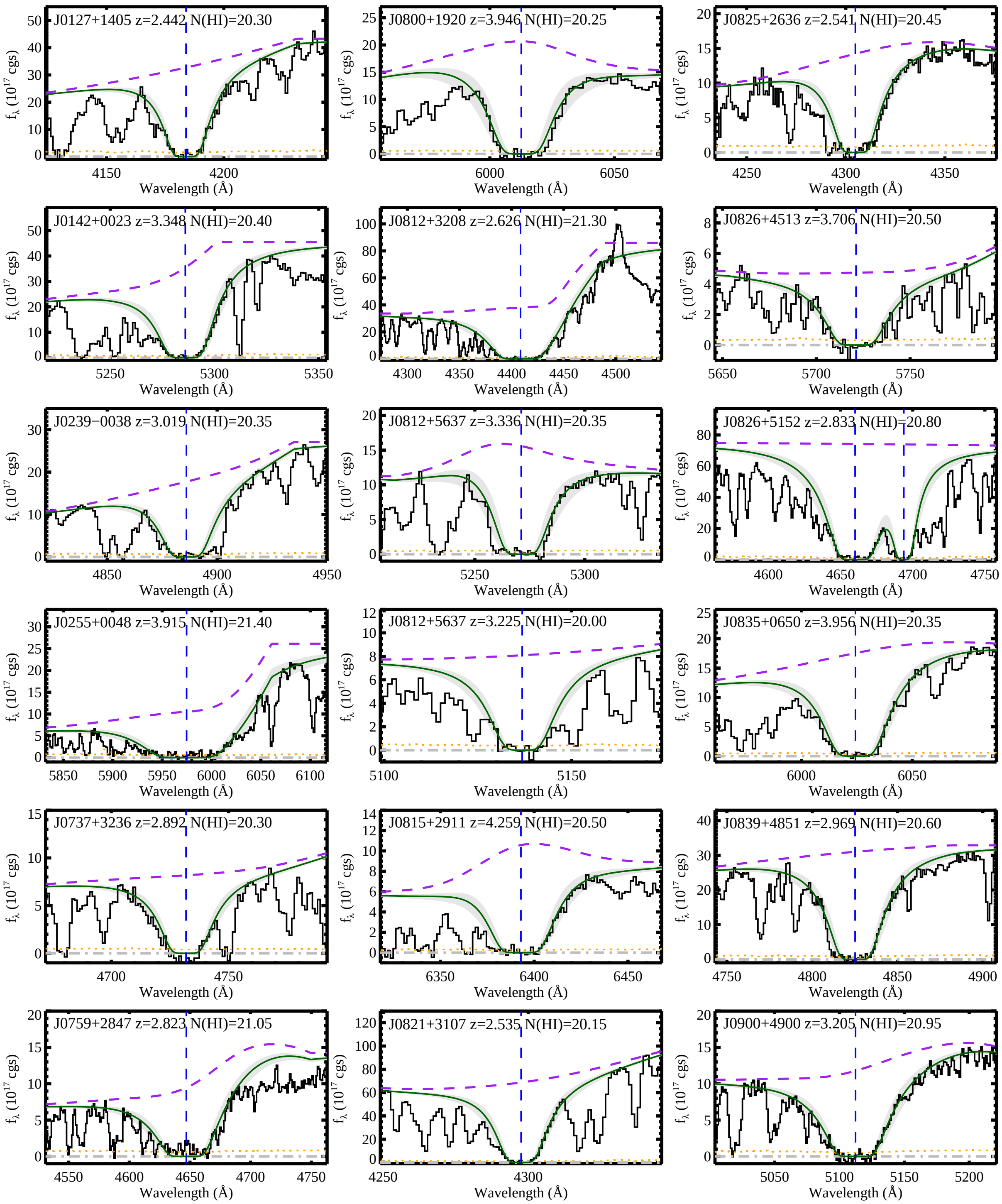

Figure A1. Fits to the Lyα absorption in our PDLA sample, the blue vertical dashed line indicating the centre of the Lyα trough. QSO names are abbreviated to Jhhmm+ddmm in order to fit the panels. Full SDSS QSO names are given in Table 1. In cases where 2 PDLAs are present, they are shown in separate panels but have been fitted simultaneously due to the significant overlap in velocity space. The grey shaded region shows the uncertainty in the fit. The grey dot-dashed line shows the zero level and orange dotted line line the 1σ error array. The purple dashed line shows the fit to the continuum.

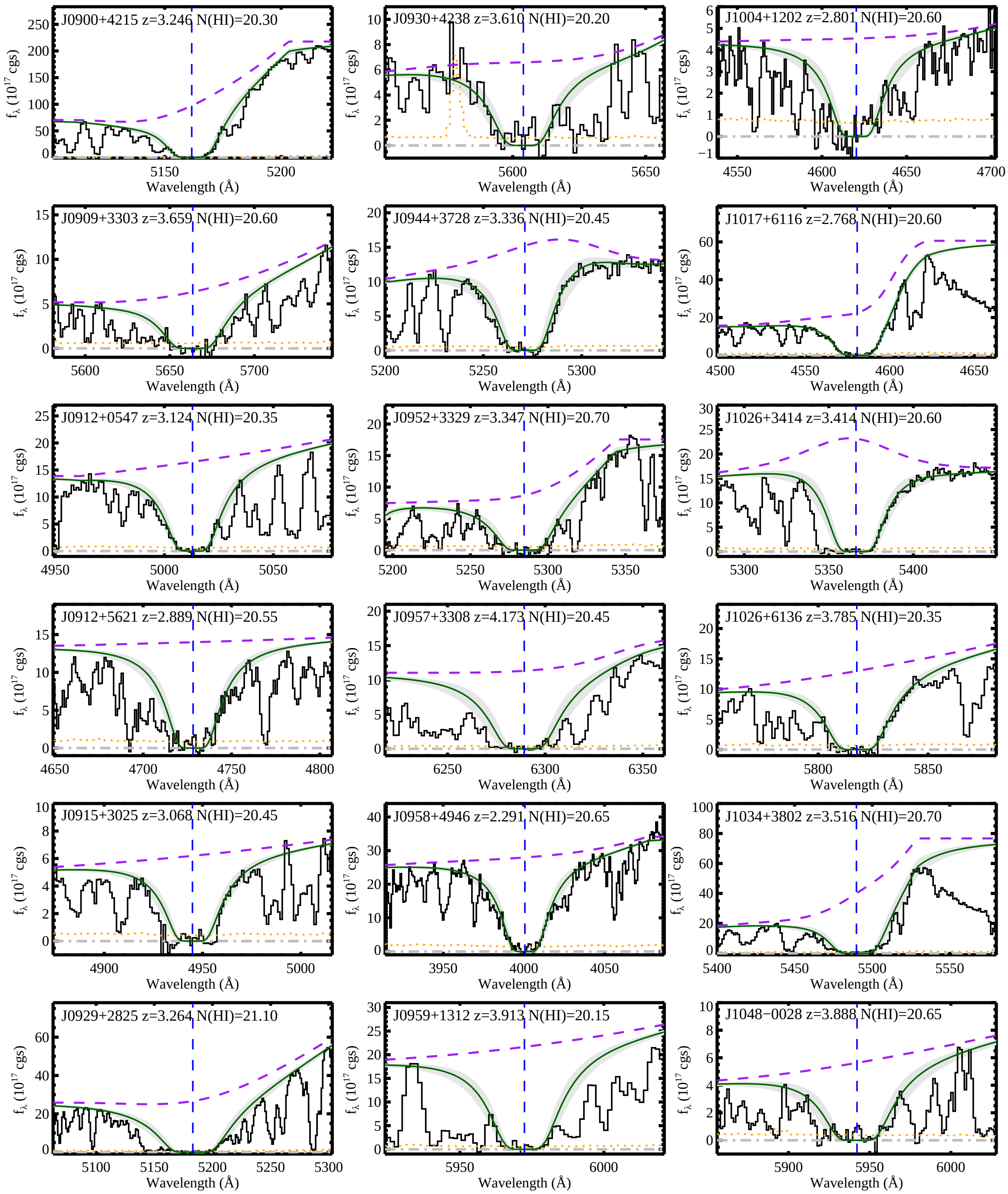

Figure A1. Continued.

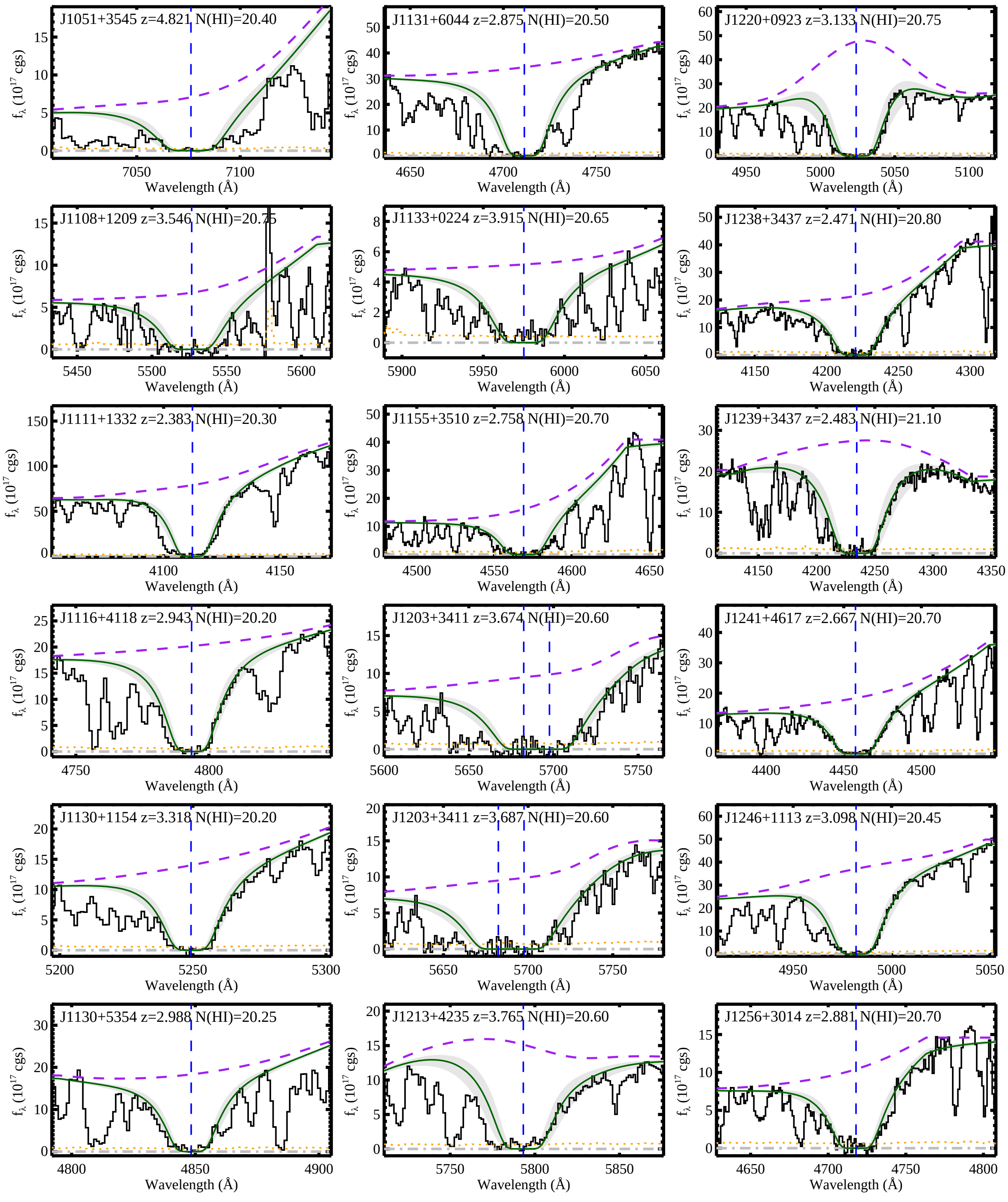

Figure A1. Continued.

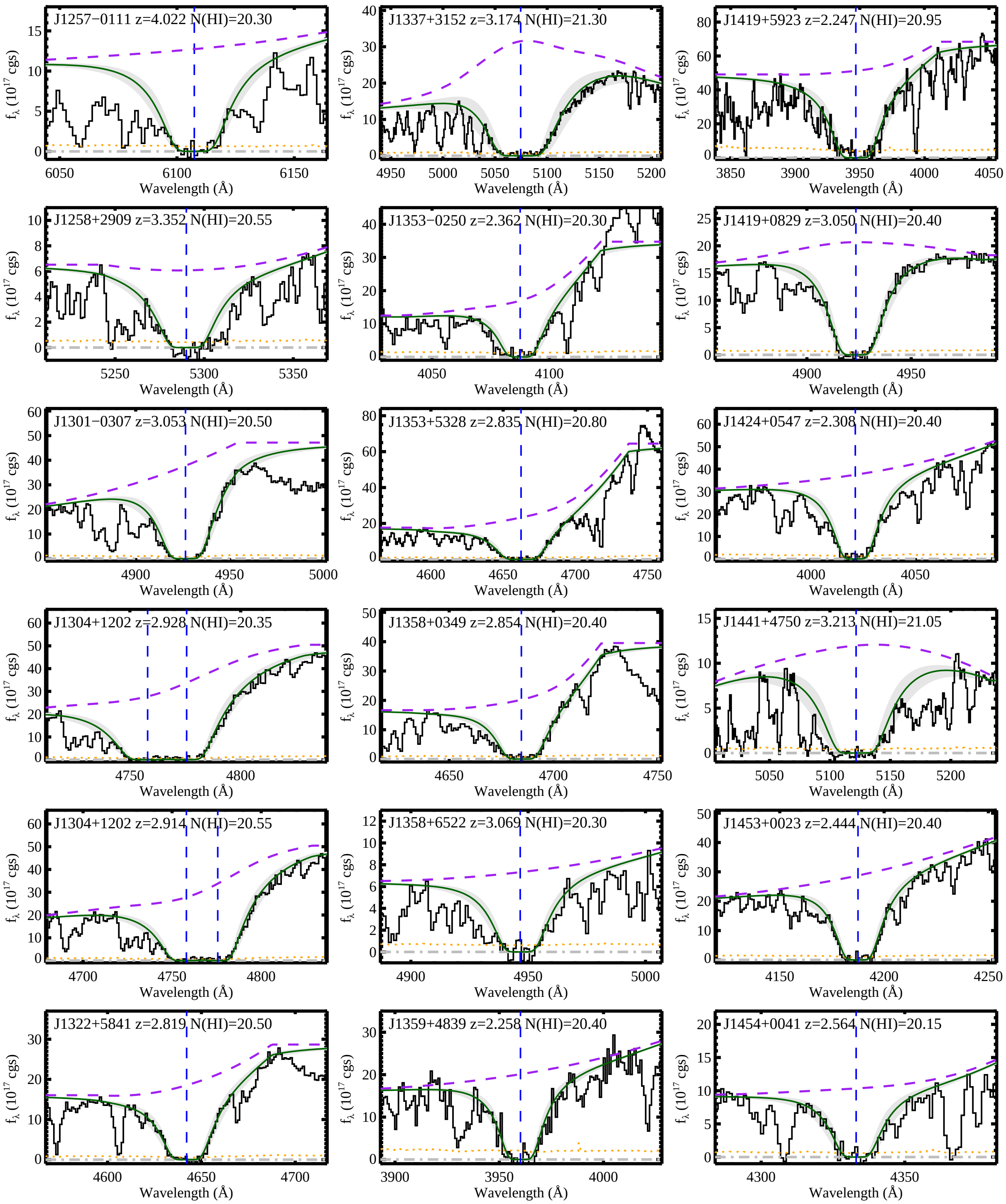

Figure A1. Continued.

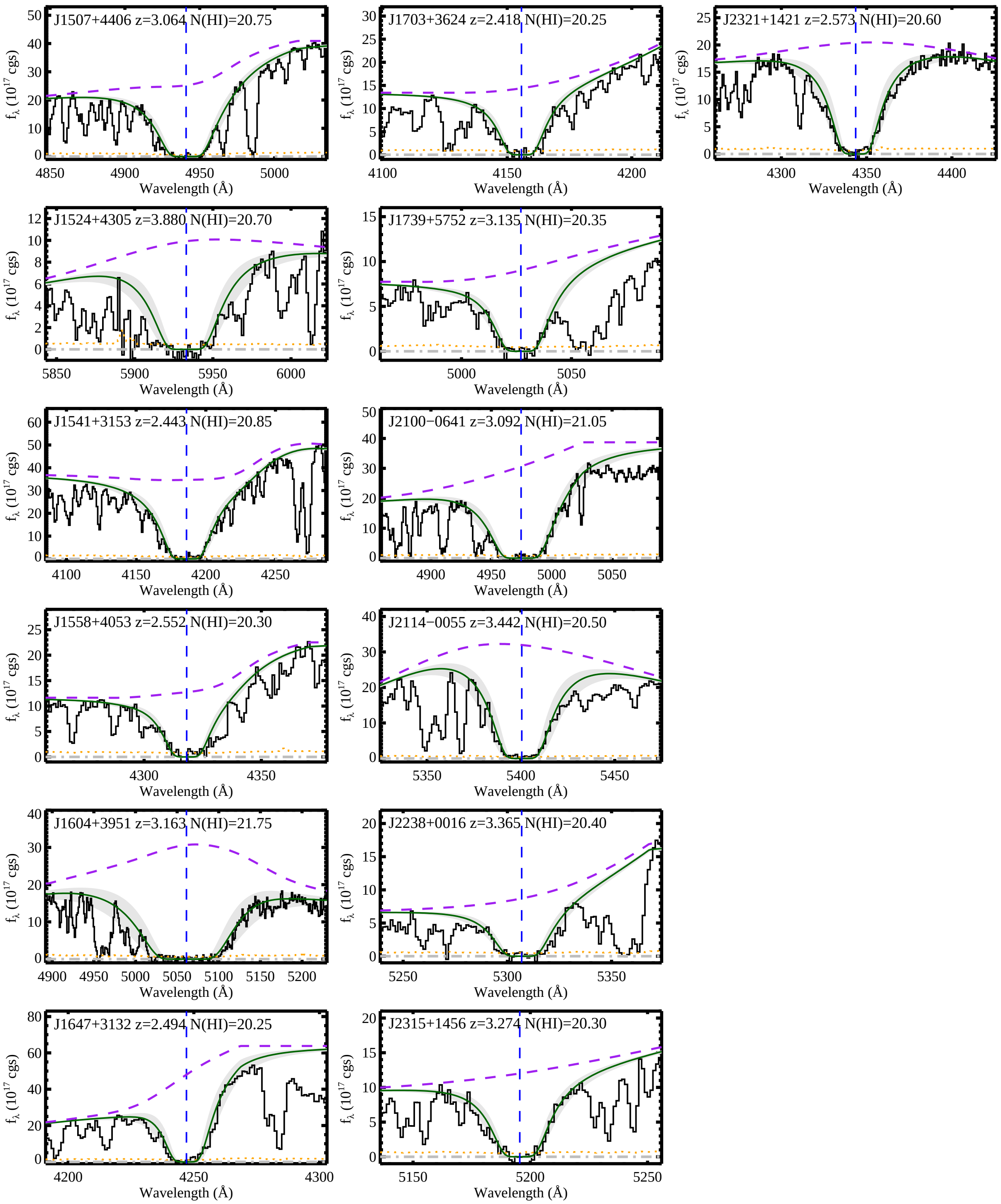

Figure A1. Continued.